

Robustness of point measurements of carbon dioxide concentration for the inference of ventilation rates in a wintertime classroom

Carolanne V. M. Vouriot^{a,b,*}, Maarten van Reeuwijk^c, Henry C. Burridge^c

^a*Department of Civil and Structural Engineering, University of Sheffield, Mappin Street, Sheffield S1 3JD, UK.*

^b*Department of Applied Mathematics and Theoretical Physics, Centre for Mathematical Sciences, University of Cambridge, Wilberforce Rd, Cambridge CB3 0WA, UK.*

^c*Department of Civil and Environmental Engineering, Skempton Building, South Kensington Campus, Imperial College London, London SW7 2BX, UK.*

Abstract

Indoor air quality in schools and classrooms is paramount for the health and well-being of pupils and staff. Carbon dioxide sensors offer a cost-effective way to assess and manage ventilation provision. However, often only a single point measurement is available which might not be representative of the CO₂ distribution within the room. A relatively generic UK classroom in wintertime is simulated using Computational Fluid Dynamics. The natural ventilation provision is driven by buoyancy through high- and low-level openings in both an opposite-ended or single-ended configuration, in which only the horizontal location of the high-level vent is modified. CO₂ is modelled as a passive scalar and is shown not to be ‘well-mixed’ within the space. Perhaps surprisingly, the single-ended configuration leads to a ‘more efficient’ ventilation, with lower average CO₂ concentration. Measurements taken near the walls, often the location of CO₂ sensors, are compared with those made throughout the classroom and found to be more representative of the ventilation rate if made above the breathing zone. These findings are robust with respect to ventilation flow rates and to the flow patterns observed, which were tested by varying the effective vent areas and the ratio of the vent areas.

Keywords: CO₂ sensors; UK schools; Indoor air quality; Computational Fluid Dynamics; Natural ventilation

1. Introduction

Eleven million pupils and school staff in the United Kingdom spend a significant proportion of their time in school buildings, the majority of which is in classrooms. As such, the indoor air quality of classrooms has the potential to directly affect the health of a large proportion of the population and, indirectly, their families too. Classrooms around Europe have previously been found to experience relatively low levels of ventilation with links being drawn to effects on pupils’ health, well-being and academic performance [1–4]. The COVID-19 pandemic has brought the issue of indoor air quality in schools and classrooms to the forefront of the attention of the wider public, with airborne disease transmission now a major concern.

Characterising ventilation rates is critical to understand indoor air quality and building performance, however it can be challenging to do routinely and reliably [5]. Measuring carbon dioxide (CO₂) offers a means to assess a building’s ventilation rate for long times, across years, using affordable sensors that are becoming widespread. In classrooms, in the absence of other combustion sources, occupants are the main source of CO₂ through their exhaled breath. High CO₂ concentration is likely to indicate poor ventilation and therefore a likely accumulation of other pollutants, including infected breath. In a single room, CO₂ can also be used as a naturally-occurring tracer gas to measure the ventilation rate, using for instance build up, steady state or decay methods [6], all of which have been used in classrooms as reviewed by Batterman [7] and by Kabirikopaei and Lau [8]. Estimating ventilation rates from CO₂ measurements relies on a number of assumptions [9, 10], including: assuming that the CO₂ generation rate is known, which requires knowing the number of occupants and their activity level; as well as, assuming that each room is a well-mixed single zone so that the CO₂ concentration is uniform and that it can be measured by a single sensor. Previous measurement campaigns in schools and standards have provided differing

*Corresponding author

Email address: c.v.vouriot@sheffield.ac.uk (Carolanne V. M. Vouriot)

recommendations for sensor placement [11], an inconsistency that is likely exacerbated by the considerable CO₂ variations measured in classrooms by both Mahyuddin et al. [12] and Zhang et al. [11]. This is especially problematic for naturally ventilated spaces, where the ventilation is not mechanically driven and thermal stratification can be expected to arise. Since the majority of UK classrooms are naturally ventilated, with more than 90% of energy display certificates issued for school buildings in England and Wales from October 2008 to June 2021 describing their ventilation system as natural ventilation [13], it is necessary to understand whether a single CO₂ measurement can accurately represent the ventilating flow supplied to the classroom, and by extension, the resulting exposure to contaminants indoors and potential infection risk of the occupants.

In this work, the effect of the ventilating flow on the CO₂ distribution and the resulting accuracy of the estimate of the ventilation rate are assessed using Computational Fluid Dynamics (CFD). In such simulations, the ventilating flow rate can be directly measured and compared to the estimate obtained from CO₂ measurements, which is rarely, if ever, achieved in operational classrooms. In addition, with CFD, the specific effects of the ventilation provision on the CO₂ spatial distribution can be determined without other confounding factors (like sensor accuracy or changes in occupancy levels) which are inevitable in field measurements. Choice is made herein to focus on a steady state method where the CO₂ concentration is assumed to have reached a steady level before calculating the ventilation rate. This choice was made for several reasons, although it is acknowledged that, quite often, in operational classrooms the timescales are such that a steady CO₂ concentration might only be expected to be reached after several hours and so practical observations are challenging. One reason for the choice is that primary school classrooms are the focus and, in the UK, they can be assumed to host school children for longer periods, increasing the chance of reaching a steady state. Considering a steady state scenario does not need a representative timetable for the pupils, which might differ between schools and classrooms. Using a decay method for instance, requires knowledge of when all occupants leave the room and, in addition, assumes that the ventilation rate assessed during unoccupied hours is the same as that during occupied hours, which for naturally ventilated classrooms (typical in the UK) is not likely to be the case [7]. Although it can overestimate the ventilation rate [14], the steady state method is often used in schools and Kabirikopaei and Lau [8] have shown that it is the method with the lowest uncertainty. Assuming the measured peak concentration value to indicate the steady value, as illustrated by Haverinen-Shaughnessy et al. [1] for instance, also gives an upper bound for the ventilation provision and is useful to identify spaces with insufficient ventilation. Finally, by considering a steady state scenario, the spatial variations in CO₂ concentration can be isolated from transient effects to comprehensibly determine how they are affected by the ventilation provision. For these reasons, we herein simulate rooms in steady state.

The reference scenario considered herein is one driven by horizontal convection which has been observed both experimentally and numerically in spaces with a distributed buoyancy source [15]. This paper aims to assess whether for the reference scenario considered here, in which the ventilation is buoyancy driven through low and high-level vents and convection is assumed to be the dominant source of heat transfer, the CO₂ concentration can be assumed to be well-mixed, and if not then: what is the degree of uncertainty that is introduced by assuming the air in the classroom is well-mixed? To inform the potential variability within a classroom, two limiting ventilation configurations are investigated. Between the two configurations the horizontal location of the top opening on the ceiling is changed: in one configuration, a flow from one end of the classroom to the other is promoted, herein the ‘opposite-ended’ configuration; and in the other, both vents are positioned at one end of the classroom, herein the ‘single-ended’ configuration. The impact of the ventilating flow rate on the results is also assessed, varying the size of the openings to either restrict or enhance the flow, as well as the effect of the ratio of the areas of the high- and low-level vents. In practice, many CO₂ sensors are deployed by attaching them to walls (a viable choice from many perspectives) but the extent to which these measurements might be representative of the CO₂ concentration within the bulk of the space, and particularly in the breathing zone, is not known. As such, this paper also investigates the degree of any additional uncertainties introduced when point measurements of CO₂ are taken near the walls; in addition the sensitivity of the CO₂ measurements to height is also investigated.

The methodology is introduced in §2. §3 compares the opposite-ended and single-ended configurations for a reference scenario: the resulting ventilating flow is described, the CO₂ concentration in the room and in the breathing zone are compared and the impact of using wall measurements is also discussed. In §4, the reference set-up is modified to investigate the sensitivity of the previous results to changes in the ventilating flow rate by varying the low and high-level vent areas. §5 details how the inferred ventilation rate is affected by the location of the CO₂ measurement when compared to the other uncertainties associated with estimating the ventilation provision. Finally, conclusions are drawn in §6.

2. Methodology

The basis of this study are CFD simulations of the Reynolds averaged Navier-Stokes equations within an idealised naturally ventilated classroom during wintertime that were described in detail in Vouriot et al. [15]. The numerical simulations investigate an idealised model of a classroom which replicates certain aspects broadly representative of a typical naturally ventilated UK classroom and the objective here is to extend these simulations with CO₂ emissions in order to provide estimates of CO₂ exposure within the expected order of magnitude. A single classroom is simulated with ventilation openings at low- and high-level (Figure 1), and the heat losses at the walls, air leakage, radiative effects and thermal mass are neglected. The effects of the openings are considered only through the ventilating flow they provide. These openings are modelled as flat open surfaces on the floor and ceiling of the room, therefore also avoiding the consideration of bi-directional flows through the ventilation openings. Using floor and ceiling openings is expected to be broadly representative of most buoyancy dominated ventilation flows with high- and low-level openings, irrespective of their precise orientation [16]. We note that beyond buoyancy-dominated ventilation flows, wind can have significant effect, either opposing the flow [17] or enhancing mixing [18], but the incorporation of these effects remain the focus of future research.

A wintertime scenario is considered as it corresponds to the time of year during which classrooms might be least ventilated and have been shown to exhibit the highest concentrations of CO₂ [19]. Although classrooms are subject to a wide variety of heat sources, we pursue a lumped approach here and apply all heat inputs (heaters, people, solar gains, electronic devices) to the floor area. Following similar reasoning, the CO₂ input is also approximated by the addition of a passive tracer uniformly distributed over the classroom’s cross-section, which is deemed appropriate to densely occupied spaces such as classrooms, and released steadily at breathing height. This, again, is a simplification since the release of human breath is both buoyant and periodic. These effects are important in the near-field, but the focus of this study is the far-field where the injection method is less important.

Initially, two ventilation configurations are investigated. In each of these, the opening areas, heat input and therefore overall flow rate are kept constant but the position of the top vent is changed leading to:

- an opposite-ended configuration with vents at opposite ends of the room, and
- a single-ended configuration with vents on the same end of the room.

The heat input from radiators in the room is adjusted to enable the provision of a comfortable thermal environment to the pupils and staff. The focus is on a primary school classroom as younger children are more vulnerable to indoor contaminants and therefore a more at risk population. The occupants of the classroom are assumed to be of primary school age (between the ages of 5 and 11 in the UK) when defining their CO₂ and heat outputs. The occupants’ breathing is modelled as a steady volumetric source of CO₂, represented by the addition of a continuous planar release of a passive scalar at breathing height (set here to be between 1.1 and 1.2 m, the typical breathing height of seated primary school pupils from the BB101 guidance [20]).

Following these assumptions, the exact reference scenario to be simulated is selected following the available guidance. The classroom is assumed to have 32 occupants following the BB101 guidelines [20]. The classroom is sized using the minimum requirements given by BB103 [21] and also corresponds to the reference case of Jones et al. [22]: the surface area is set to 55 m², with a ceiling height of 2.7 m. An illustration of the set-up considered is shown in Figure 1. Ventilation is driven through high- and low-level openings located on the floor and ceiling of the classroom. In the initial scenario, the low-level vent has an area A_l of 0.4 m² (0.8 m × 0.5 m) centred at coordinates (1.4, 1.25, 0). Two ventilation configurations are then investigated by changing the location of the upper-level vent, while keeping its area A_h constant and equal to 0.2 m² (0.5 m × 0.4 m). In the opposite-ended (OE) configuration, it is positioned at the opposite end of the classroom from the low-level opening and centred around (8.75, 4.3, 2.7). In the single-ended (SE) configuration, the opening is positioned on the same end as the bottom opening and centred at coordinates (1.25, 4.3, 2.7). The 32 occupants in the room are each assumed to produce 60 W of heat [20] and a CO₂ generation rate of $G = 3.35 \times 10^{-6}$ m³/s, which is the average for primary aged school children aged between 6 and 11 as reported by Persily and de Jonge [23], assuming an activity level of 1.4 met (which corresponds to an increase in the child’s activity proportional to the increase in activity level of an office worker writing or standing, compared to the levels for rest). We do not explicitly account for the slightly higher CO₂ generation of the one, or two, teaching staff likely to be present in the room — the impact of such differences falls within the uncertainty of the CO₂ generation rate; for example, due to differences in activity level within the occupants. In order to be precise for any particular group of occupant, their generation rate would have to be representative of their level of activity, age and gender, all of which can lead to large variations between individuals. Since the focus on this paper

is not on the effect of the different occupants’ position on the CO₂ distribution, a consistent individual generation rate G is used and distributed uniformly across the room. An additional 4,280 W of heat is supplied at the floor to take into account the classroom heating provision and ensure a comfortable room temperature. The ambient outside temperature T_a is taken to be 5°C, assumed to be typical for the coldest months in the UK.

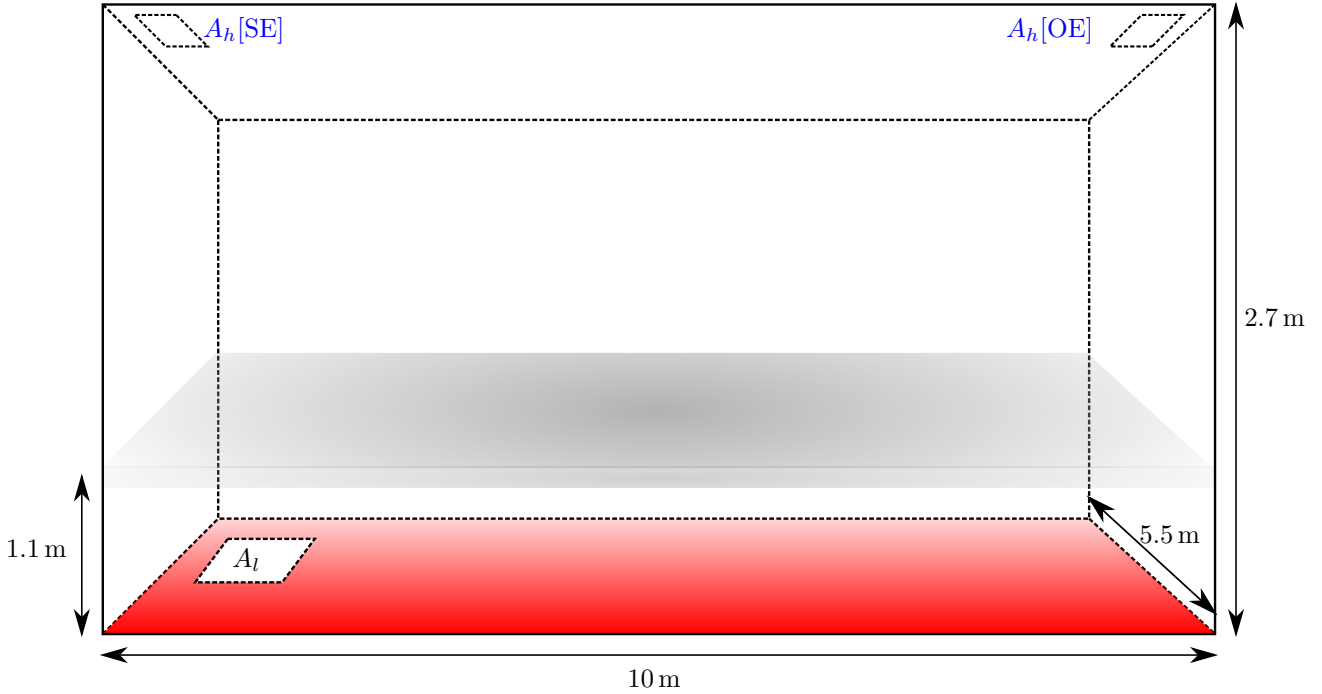


Figure 1: Illustration of the set-up used to represent a generic naturally ventilated UK classroom (either in a single-ended (SE) or opposite-ended (OE) configuration). The heat is input on the floor as shown in red here. A passive scalar representing CO₂ is introduced at breathing height (between 1.1 and 1.2 m).

The CFD simulations are run using OpenFOAMv2106, developed by OpenCFD [24]. A transient solver, `buoyantPimpleFoam`, is used due the presence of long-time period fluctuations, potentially characteristic of internal wave modes, within the data generated by steady solvers despite the absence of time-dependent or varying boundary conditions. To reduce run-times, our simulations are initialised with a stratification established by a steady run. Subsequently, the simulations are run with a transient solver for 8,600 s with statistics averaged only over the last 3,600 s. These values are chosen to ensure a suitable convergence and accuracy of the results while limiting computational costs. Overall, each simulation took approximately 15 hours to run (using 1,024 cores) on the UK National Supercomputing Service’s ARCHER2 (i.e. each simulation consumed around 15,360 cpu hours).

Simulations are run using the $k-\omega$ SST turbulence model. This model strikes a balance between the performance of $k-\epsilon$ models for shear flows and $k-\omega$ models at the walls [25], both features relevant to the capturing ventilating flows. Large variations in the turbulence levels in the classroom can also be expected [26], leading to potential relaminarisation of the flow which the $k-\omega$ SST model is expected to capture. The chosen OpenFOAM version also incorporates the effects of buoyancy on turbulence production by using the `buoyancyTurbSource` finite volume option [27].

The computational domain includes the classroom along with two exterior boxes linked to the classroom through inlets and outlets, included in order to properly model the effect of flow at the two openings and the resulting flow in the classroom, as shown in Figure 2. The classroom is defined as a cube of dimensions 10 m \times 5.5 m \times 2.7 m. The bottom exterior box is centred around the inlet to the classroom, with dimensions 2.8 m \times 2.5 m \times 1 m. The top exterior covers the same surface as the classroom with dimensions 10 m \times 5.5 m \times 3.7 m. The classroom is linked to the exterior boxes via an inlet and an outlet of the same size as the vents with respective areas A_l and A_h , and height 0.2 m. The sensitivity of the simulations to the size of the external boxes was tested and these dimensions were chosen as they did not impact the results. The mesh is defined as a perfect orthogonal mesh with $\Delta x = \Delta y = \Delta z = 0.05$ m in the classroom, inlet and outlet and $\Delta x = \Delta y = \Delta z = 0.1$ m in the exterior, leading to

Parameter	Symbol	Unit	Input
Floor surface area	S_c	m ²	55.0
Classroom volume	V_c	m ³	148.5
Classroom height	H_c	m	2.7
Number of occupants	N	-	32
Inlet area	A_l	m ²	0.40
Outlet area	A_h	m ²	0.20
Heat input	W_c	W	6200
CO ₂ generation rate	G	m ³ /s	3.35×10^{-6}
Outdoor temperature	T_a	°C	5
Outdoor CO ₂ concentration	C_a	ppm	400
Ambient density	ρ_a	kg/m ³	1.268
Thermal expansion coefficient	α	K ⁻¹	0.00362
Heat capacity	c_p	J/kg/K	1005

Table 1: Inputs used to define the classroom simulation.

1,399,356 hexahedral cells. A grid convergence study was also performed: the mesh used in this study accurately represents both the bulk flow and CO₂ distribution when compared to a finer mesh (with $\Delta x = \Delta y = \Delta z = 0.025$ m), full details are presented by Vouriot [28] and Vouriot et al. [15].

At all walls, including the classroom's and the exterior boxes' (apart from the domain inflow and outflow), a no-slip velocity boundary condition is used. All walls are also assumed to be adiabatic, with the exception of the floor where a constant 6,200 W heat input is imposed. The scalar representing the breath of occupants through the addition of CO₂ is added over the surface area of the classroom between the heights of 1.1 and 1.2 m with a source corresponding to the generation rate NG . At the domain inflow the temperature and scalar are set to ambient and at the domain outflow a Neumann boundary condition is used setting the gradient of the temperature and scalar fields to 0. Velocity boundary conditions at the inflow and outflow are calculated from the pressure field where the pressure difference $\Delta p_0 = -\rho_a g H_{domain}$ is imposed across the domain inflow and outflow. In addition, the bulk flow rate and room temperature were checked against the well-mixed predictions of Gladstone and Woods [29] (described in Appendix A) and the flow pattern arising from the distributed heat source was comparable to what was observed in small-scale experiments [15].

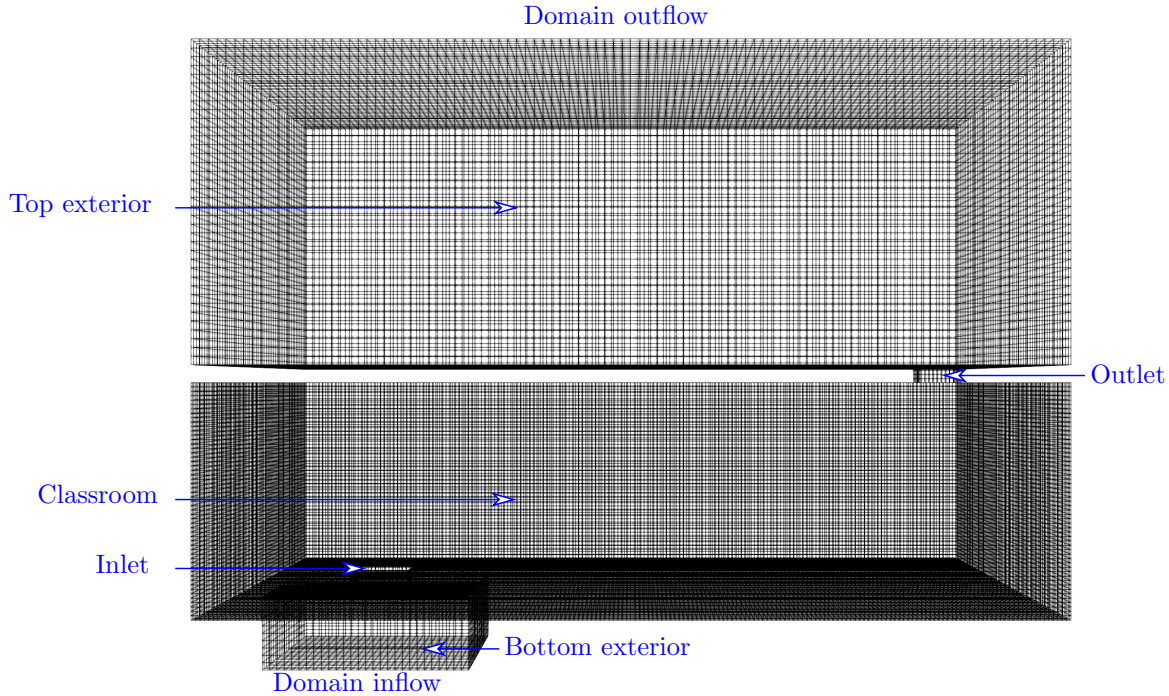


Figure 2: Computational grid used to simulate the classroom, including the modelled exterior, inlet and outlet.

3. Comparing the opposite-ended and single-ended configurations

The results of our simulations show the ventilation flow patterns differ between the opposite-ended and single-ended configurations. We report on these differences, before then evidencing the robustness of our results to different ventilation rates and the distribution of vent areas in §4.

3.1. Bulk quantities

The simulated ventilating flow rate, mean temperature, and CO₂ concentration in the classroom are given for both configurations in Table 2. The effective area A^* is 0.18 and if the discharge coefficient is taken to be identical at each vent, $c_d = c_l = c_h$, it is close to 0.7, which lies within the experimentally determined range of $0.6 \leq c_d \leq 1.0$ [29, 30]. The well-mixed predictions are presented in square brackets taking the value for the discharge coefficients c_l and c_h determined in Appendix B.

	Q (m ³ /s)	ACH (-)	Q_p (L/s/person)	ΔT (°C)	ΔT_e (°C)	ΔC (ppm)	ΔC_e (ppm)	η (-)
Opposite-ended	0.239 [0.243]	5.85 [5.90]	7.54 [7.60]	19.3 [20.0]	20.4	427 [441]	449	1.05 [1]
Single-ended	0.241 [0.247]	5.85 [5.98]	7.54 [7.71]	18.9 [19.7]	20.2	357 [435]	444	1.24 [1]

Table 2: Results of the CFD simulations for the opposite-ended and single-ended configurations, and well-mixed predictions (shown in square brackets) using the loss coefficient at the vents c_h and c_l calculated in Appendix B, for: the ventilating flow rate, the room averaged excess temperature $\Delta T = T_c - T_a$ and excess CO₂ concentration $\Delta C = C_c - C_a$. In all five cases, T_e and C_e correspond to the exhaust values calculated from the measured ventilating flow rate Q assuming a well-mixed environment, the corresponding excess temperature and CO₂ concentration are calculated from $\Delta T_e = T_e - T_a$ and $\Delta C_e = C_e - C_a$ respectively. η gives a measure of the contaminant removal efficiency.

The bulk flow rates attained from the CFD simulations for both the opposite-ended and single-ended configu-

rations are very similar, differing by only 1%. These bulk flow rates agree with the predictions from the well-mixed model to within about 3%, an appropriate accuracy for almost all applications. For both cases, Q_p , the flow rate per occupant, is close to 8 L/s/person, in line with the BB101 guidelines [20], which advises ventilation rates of 8–9 L/s/person to achieve CO₂ concentrations of 1,000 ppm in a typical classroom.

Table 2 shows that there is only a slight difference in the room averaged excess temperature ΔT between the two configurations. Unsurprisingly, both values are quite close to the well-mixed predictions as expected given the similarities in flow rate and enforcing conservation of energy in the steady state. In addition, temperature is an active tracer such that variations in a horizontal plane result in buoyancy forces which act to promote mixing. Conversely, for the case of the room-averaged excess CO₂ concentration ΔC (which is a passive tracer within the simulations), the difference between the two simulations is around 16%. Interestingly, the average CO₂ concentration in the single-ended configuration is *lower* than in the opposite-ended configuration. This indicates, perhaps counter-intuitively, that if one takes CO₂ concentration as an indoor air quality indicator, then the single-ended ventilation could be considered as having better indoor air quality. We investigate this finding in more detail below.

The differences between the two configurations, and the extent to which the well-mixed predictions presented in Appendix A are appropriate, are investigated by calculating the expected exhaust temperature T_e by rearranging eq. (4) and eq. (6), and CO₂ concentration C_e from eq. (7), using the flow rate Q obtained numerically. This enables the contaminant removal efficiency, η , to be examined — this metric has frequently been used to analyse the performance of ventilation configurations [e.g. 31, 32], and we define

$$\eta = \frac{\Delta C_e}{\Delta C} = \frac{C_e - C_a}{C_c - C_a}. \quad (1)$$

Although similar to the ventilation efficiency or effectiveness defined by Sandberg [33] and used, for instance, by ASHRAE [34], here the contaminant is not introduced at the inlet but generated within the room. If η is equal to unity, the efficiency is equivalent to the one found in a perfectly mixed room. Values below unity indicate short-circuiting and values superior to unity are representative of displacement ventilation systems [32]. For the single-ended simulation, the contaminant removal efficiency is found to be equal to 1.24 and indicative of the performance of displacement ventilation. Practically, this implies that if the room averaged CO₂ concentration C_c were used to predict the ventilation rate, the ventilation rate would be overestimated, in this case by 24%. In the opposite-ended configuration, although still superior to unity (with $\eta = 1.05$), η is a lot closer to the efficiency expected in a perfectly well-mixed room and indicative of a less effective ventilation configuration than the single-ended configuration.

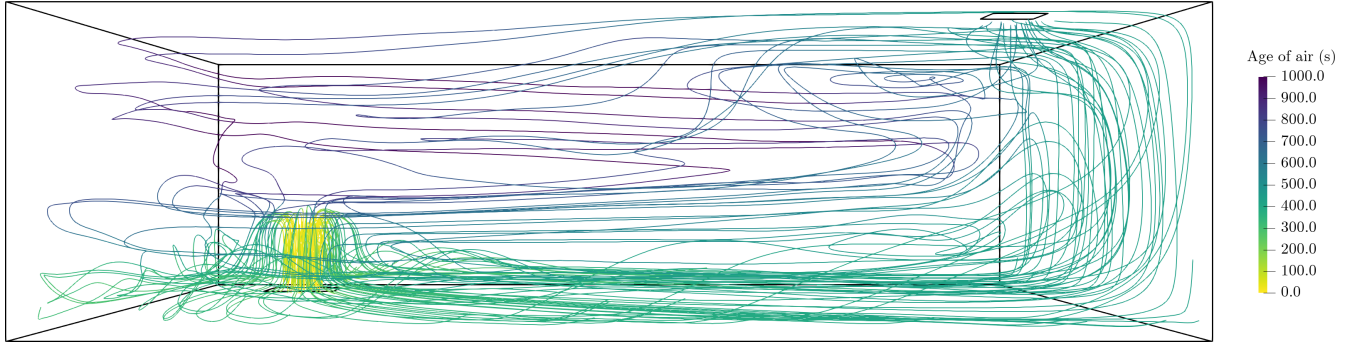
3.2. Flow pattern and vertical variations

To better understand the factors underlying the difference in performance of the two configurations, the flow pattern is investigated via the study of the streamlines within the classroom. Figure 3a) and Figure 3b) show the pattern of the ventilating flow for the opposite-ended and single-ended configurations, respectively. In each case, the streamlines are coloured by the age of air — a statistic which represents, the time that air at a given point in the room has been within the room, and hence gives a measure of the ‘freshness’ of the air.

In both configurations, the incoming cold air can be seen flowing into the classroom through the low-level vent, forming a fountain [35], and falling back down to the floor. This relatively cold air then flows along the floor across the room before hitting the opposite wall and flowing upwards. In the opposite-ended configuration (Figure 3a), the flow partially leaves the classroom directly through the high-level vent. In the single-ended configuration however (Figure 3b), the air then flows along the ceiling before reaching the classroom outlet on the other side of the classroom. Figure 3b) shows that the single-ended configuration does not lead to short-circuiting, and, on the contrary, creates a ventilating flow that covers a large proportion of the classroom. On the other hand, Figure 3a) shows a large area of the room away from the outlet in the opposite-ended configuration in which there is little ventilating flow. This area contains relatively stale air, and likely leads to an accumulation of CO₂ concentration, therefore increasing the overall room average. This is of concern for exposures since this region of stagnating air is located within the breathing zone. This investigation of the streamlines, and associated age of air, sheds light on the differences in the flow patterns between the two configurations which give rise to, and were evidenced by, the differences in the bulk metrics for each configuration as shown by Table 2.

The differences in the ventilating pattern between the two configurations is also visible in the horizontally averaged excess temperature and CO₂ concentration (see Figure 4). The horizontally averaged excess temperature (Figure 4a) increases with height, from about 14°C near the floor to over 20°C near the ceiling. Below a height of

a) OE



b) SE

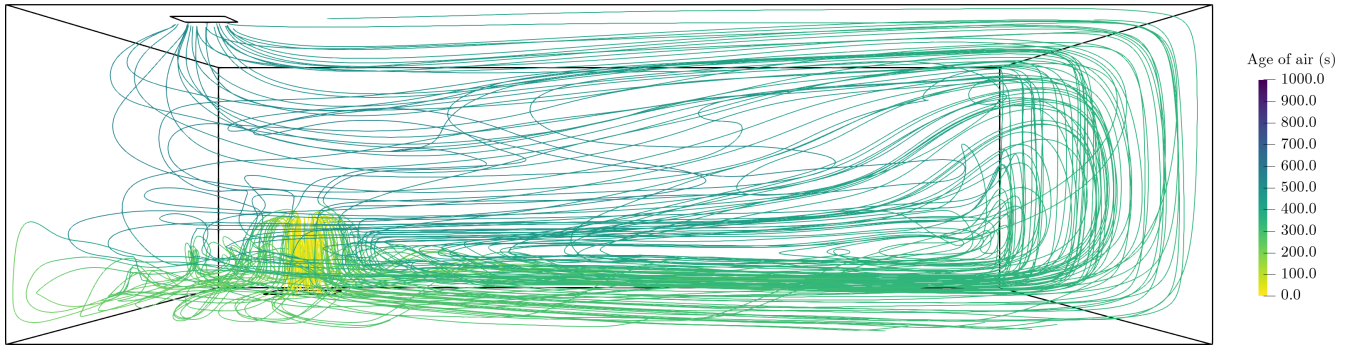


Figure 3: Streamlines originating from the low-level vent in both a) the opposite-ended and b) single-ended configurations coloured by the age of air. In both cases, 100 streamlines are seeded at the classroom inlet.

0.75 m, both ventilation configurations exhibit notionally identical temperatures, but higher up the opposite-ended configuration exhibits elevated horizontally averaged excess temperatures, by around 1°C . Defining the heat removal efficiency as $\Delta T_e/\Delta T$ (equivalent to the definition of η), results in values of 1.06 for the opposite-ended and 1.07 for the single-ended configurations, which are close to a well-mixed environment. The differences in removal efficiency of CO_2 between the configurations, compared to the one determined for temperature, are likely due to one being a passive and the other an active scalar, as discussed previously.

The similarity in temperature profiles is in contrast to Figure 4b) which shows the horizontally averaged excess CO_2 concentration in the classroom. Both configurations exhibit a significant variation in CO_2 concentration with height which broadly follow a similar profile shape in which the CO_2 concentration peaks within the breathing zone (1.0 m–1.5 m) where CO_2 is introduced. However, the CO_2 concentration is higher in the opposite-ended scenario, than the single-ended, at all heights. We note that whilst the opposite-ended configuration contaminant removal efficiency is found to be close to a well-mixed value ($\eta = 1$), this occurs in the presence of significant vertical variations in the horizontally averaged CO_2 concentration around the well-mixed value, it just so happens that in this case the variations approximately sum to zero — there is no requirement that this is inherently the case, as illustrated by the findings for the single-ended configuration.

Figure 5 shows the CO_2 concentration variation across the room, averaged over the height of the breathing zone. Both configurations, exhibit significant variations around the well-mixed CO_2 concentration (≈ 840 ppm). In particular, for the single-ended configuration, the concentration is shown to vary from around 700 to 1,400 ppm, with the lowest concentration found in the region of the rising flow (see Figure 3). This is also observed in Figure 5b), for the single-ended configuration, although the CO_2 variations are lower, only spanning the range 700 to 1,000 ppm. This difference in the distribution of CO_2 in the breathing zone can be attributed to the different ventilating patterns (Figure 3) and the mechanisms underlying these different patterns are discussed by Vouriot et al. [15].

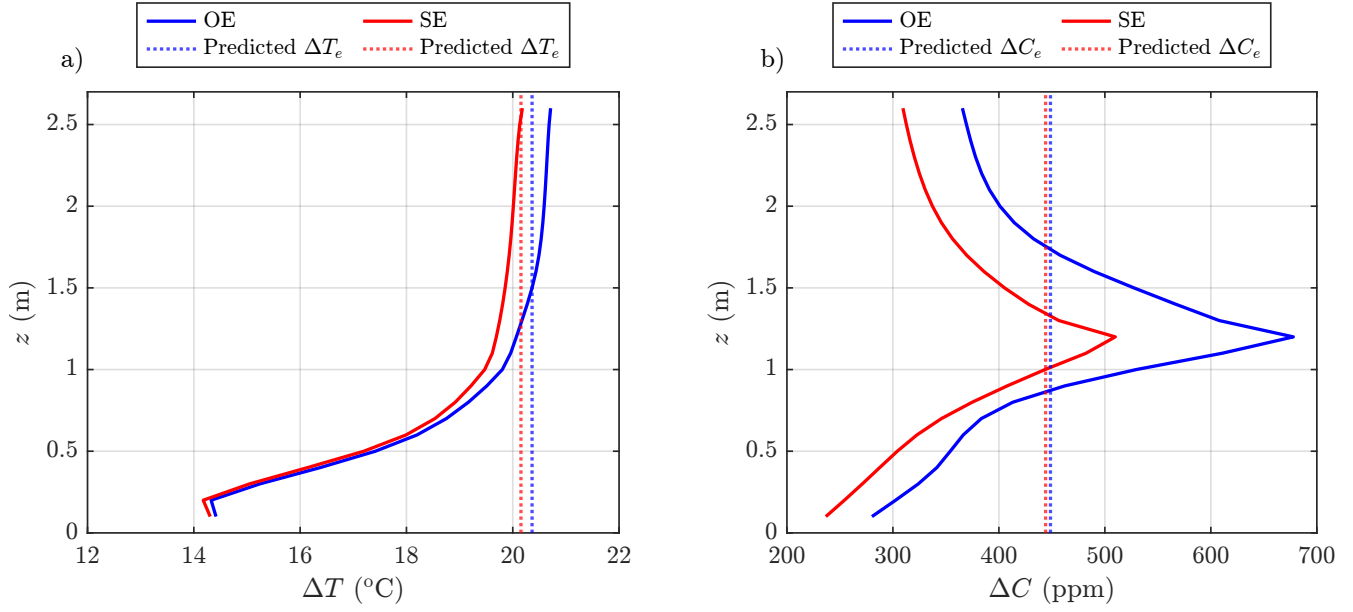


Figure 4: Horizontally averaged excess: a) temperature and b) CO₂ concentration in the classroom for the opposite-ended (OE) and single-ended (SE) configurations. ΔT_e and ΔC_e are the predicted excess exhaust temperature and CO₂ concentration calculated from the measured flow rate.

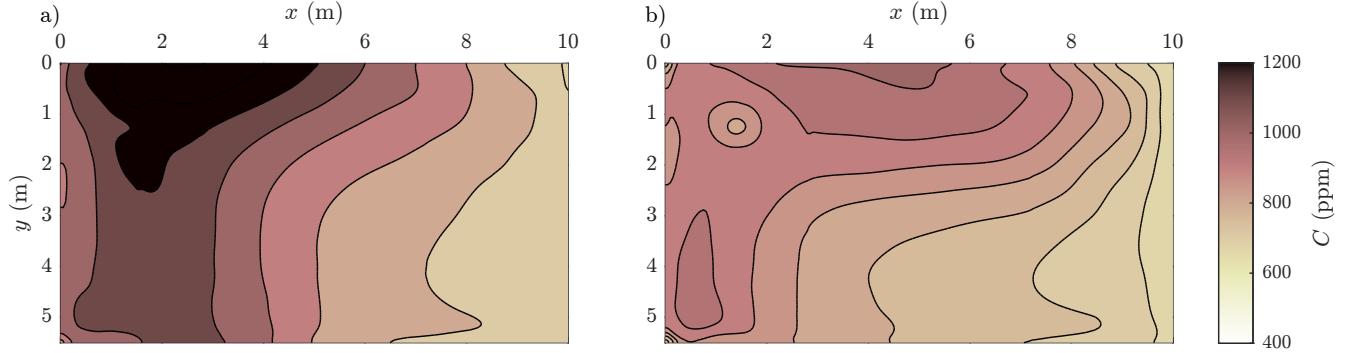


Figure 5: Horizontal cross section of the CO₂ concentration, vertically averaged, in the breathing zone ($1 \leq z \leq 1.5$ m) for: a) the opposite-ended and b) the single-ended configuration.

3.3. CO₂ spatial distribution

Given the significant differences between the two ventilation configurations, and its relevance as an indicator of indoor air quality, the CO₂ distribution is examined more closely in each ventilation configuration by looking at a wider variety of statistics. Table 3 compares the CO₂ distribution in the breathing zone ($1 \leq z \leq 1.5$ m) and the overall classroom, by reporting values for the mean CO₂ concentration and the coefficient of variation in each region. The coefficient of variation of the CO₂ concentration, $cVar$, is calculated in each domain by dividing the unbiased estimate of the standard deviation by the mean. The mean CO₂ concentration in the breathing zone is higher than for the overall classroom by 13% for the single-ended configuration, and 20% for the opposite ended. This increase is not unexpected given that the CO₂ is generated in this zone. What may be notable when looking at occupants' exposures, is that in the breathing zone for the opposite-ended configuration, the mean CO₂ is 17% (about one standard deviation) higher than in the single-ended configuration, and the coefficient of variation is also significantly increased.

Histograms of the distribution of CO₂ in both configurations are also shown in Figure 6: a) for the entire classroom, and b) in the breathing zone only. For reference the median values and interquartile ranges are marked by solid and dashed vertical lines respectively. All four distributions are skewed with large tails towards higher

Configuration	Location	C (ppm)	$cVar$ (%)
Opposite-ended	Classroom	827	16.6
	Breathing zone	986	18.7
Single-ended	Classroom	757	11.5
	Breathing zone	852	11.7

Table 3: Statistics of the CO₂ concentration for the overall classroom and the breathing zone ($1 \leq z \leq 1.5$ m) in the two ventilation configurations. C is the mean CO₂ concentration in each domain and the coefficient of variation $cVar$ is the ratio of the unbiased estimate of the standard deviation relative to the mean.

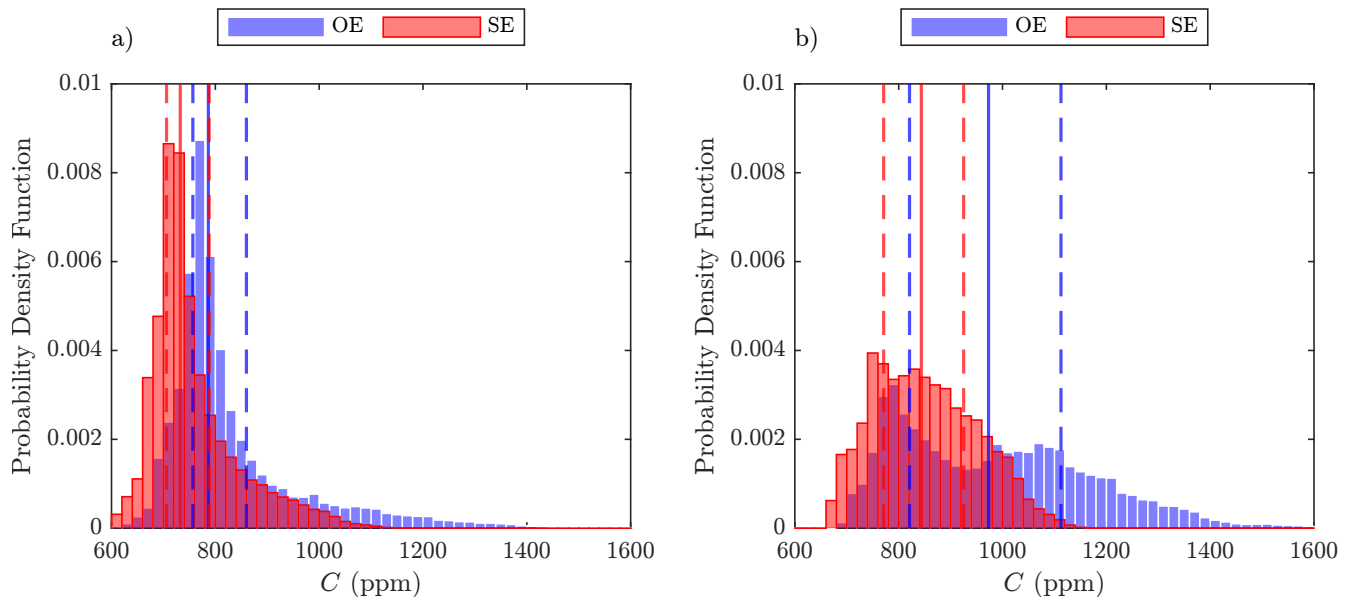


Figure 6: Histogram of the CO₂ concentration for the opposite-ended and single-ended configuration for: a) the whole classroom and b) the breathing zone ($1 \leq z \leq 1.5$ m) using 50 bins. For each case, the median is shown with a full vertical line, the first and third quartiles are shown with dashed vertical lines.

CO₂ values and in both regions, higher values of CO₂ are present in the opposite-ended configuration. Figure 6b) evidences that the values within the breathing zone are significantly elevated and are bimodally distributed in the case of the opposite-ended configuration. The breadth of the CO₂ distributions, particularly in the breathing zone, highlight potential challenges in representing or estimating exposures with a limited number of point measurements, typical of existing sensing technologies.

3.4. Sensor placement

The simulations presented here provide access to the full three dimensional fields in the classroom; we exploit this to assess where CO₂ sensors can be placed in order to take measurements of greater relevance to occupants. In particular, we analyse the CO₂ concentrations within the room as a whole and compare these to the concentrations measured only near the walls, since sensors placement is often restricted to walls — in our case taken to be within a region 0.2 m from the walls. Histograms of the CO₂ distribution at different heights are plotted for the opposite-ended and single-ended configurations (Figure 7). The greatest variation is observed in the breathing zone, e.g. $z = 1.1$ m. At the lower heights shown, differences are evident between the CO₂ concentrations in that plane and those measured at the walls. Although the mean and median values typically agree quite well, differences in some of the interquartile values highlight the changes in the distributions. However, since the flow enters at low-level and exits at high-level, and, as the flow evolves it can only mix, in both of the configurations examined, measurements above the breathing zone result in greater agreement between measurements in the plane and at the walls. If CO₂ measurements at the walls are to be used to estimate a ventilating flow rate, measurements taken above the breathing zone are found to be more likely to give accurate readings. This is increasingly true at heights above

1.9 m, and it can be assumed that this result is likely to hold for ventilation designs promoting inflows at low-level and outflows at high-level as long as measurements are never made above the height of the high-level outlet vent(s).

Simulation	At height	ϵ (%)	$cVar$ (%)	$cVar_w$ (%)
Opposite-ended	$z = 1.1$ m	2.9	20.4	23.9
	$z = 1.9$ m	1.7	5.1	8.1
Single-ended	$z = 1.1$ m	2.5	13.0	16.7
	$z = 1.9$ m	0.4	3.3	4.7

Table 4: Accuracy of the CO₂ measurements at the walls at two heights for the two ventilation configurations. ϵ is the error in the predicted mean when considering the CO₂ concentration near the walls (defined as within 0.2 m of a wall). $cVar$ is the coefficient of variation of the CO₂ concentration over the whole room at a given height and $cVar_w$ quantifies the coefficient of variation at the same height considering measurements near the walls only.

Table 4 summarises these results by comparing statistical results at heights 1.1 m and 1.9 m. The wall-error, ϵ , is first calculated to quantify the error in the average predictions made based on measurements in the wall region compared with the average of the cross section at that height, namely

$$\epsilon = \frac{|\langle C_w \rangle - \langle C \rangle|}{\langle C \rangle}, \quad (2)$$

where $\langle C_w \rangle$ is the mean CO₂ concentration at a given height measured near the walls and $\langle C \rangle$ is the mean CO₂ concentration across the whole room at that height. The table shows that whilst the difference in the wall-error is approximately doubled when measurements are made at $z = 1.1$ m, the wall-error is small, i.e. less than the measurement error for typical low cost non-dispersive infrared sensors. However, the coefficients of variations highlight that since a low number of (often single) point measurements are made within a given space, then, for these types of ventilation designs, measurements made higher up are more prudent.

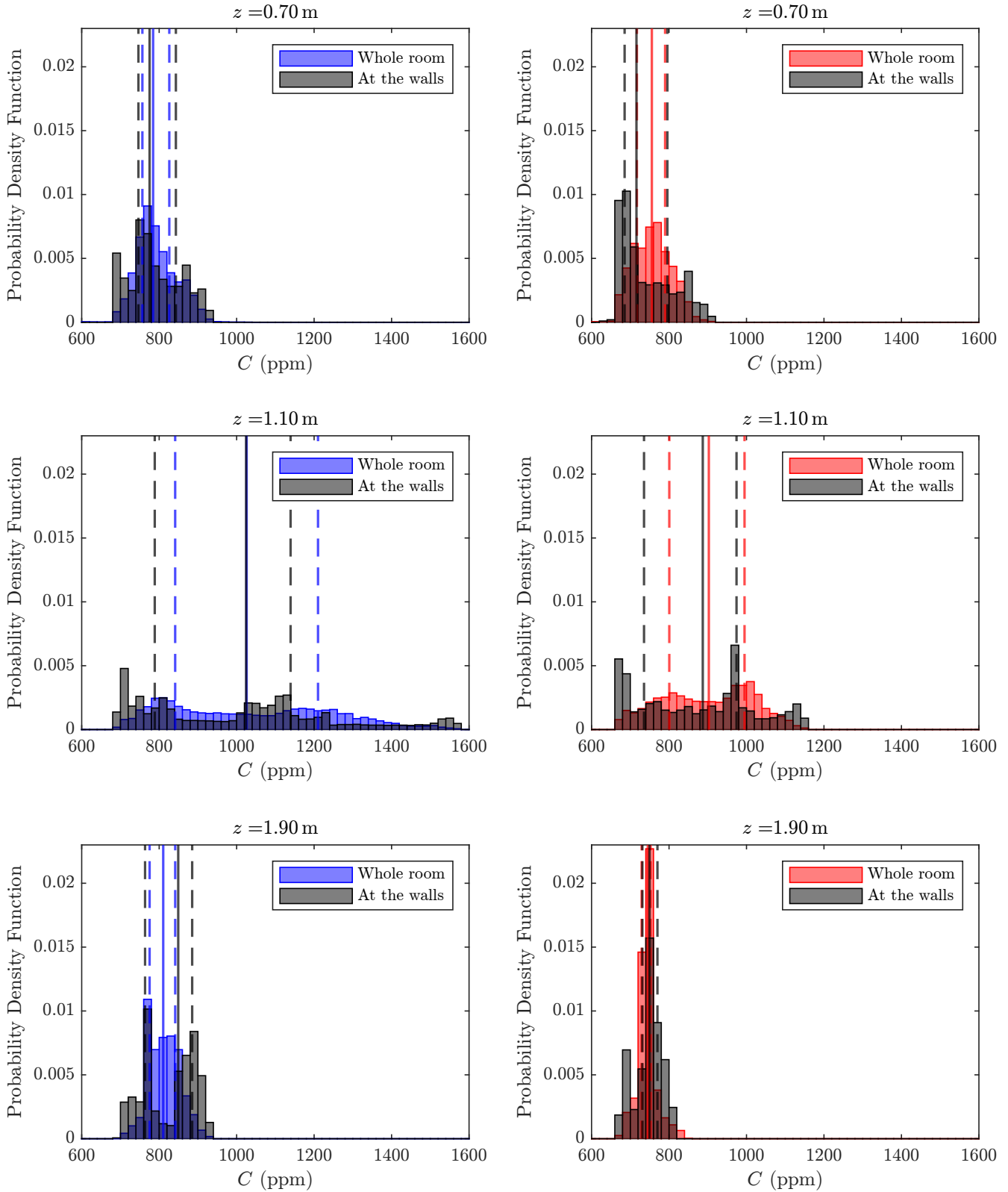


Figure 7: Histogram of the CO₂ concentration for the opposite-ended (left) and single-ended configurations (right) at three heights using 50 bins. The CO₂ concentration across the whole room at every height is compared to measurements at the walls (defined as within 0.2 m of a wall). For each case, the median is shown with a full vertical line, the first and third quartiles are shown with dashed vertical lines.

4. Sensitivity of the ventilating flow and indoor environment to different ventilation rates and distribution of vent areas

In this section, a range of different vent areas and vent area ratios are selected to investigate how robust our results might be. The different simulations selected to perform this analysis and are summarised in Table 5. The reference set-up analysed above (§3) is included and described as the original vent set-up (denoted, ‘OS’). The effective areas of the classroom openings are varied: they are reduced in simulations SO and SOR, and enlarged in the LO and LOR configurations. In the smaller openings (SO) set-up, both the inlet and outlet areas are halved and they are both doubled in the larger openings (LO) case — thus keeping the vent area ratio, A_l/A_h , unchanged. This is not the case for the SOR and LOR configurations, where only the area of the high-level vent is changed to achieve effective vent areas A^* equivalent to those calculated for the SO and LO cases respectively (*a priori* needing to assume that the discharge coefficients remain unchanged). The SOR case corresponds to a scenario with smaller openings where the vent area ratio is halved and the LOR case is a set-up with larger openings where the vent area ratio is quadrupled.

4.1. Bulk quantities and flow pattern

The bulk flow rates, room averaged temperatures and CO₂ concentrations within the classroom are given in Table 5 for each simulation and ventilation configuration. Broadly, the flow rates obtained are close to that predicted using the well-mixed predictions summarised in square brackets in Table 5 and calculated using the discharge coefficient c_l and c_h (given for each case in Appendix B). Single-ended configurations consistently lead to larger flow rates, in accordance with the discussion in §3; these differences are reduced (sometimes unnoticeable to the two decimal places reported) for cases with smaller openings that result in lower ventilation flow rates (SO and SOR).

Case	Vents	A_h/A_l	A^* (m ²)	ACH		Q_p (L/s/pers.)		ΔT (°C)		ΔT_e (°C)	ΔC (ppm)		ΔC_e (ppm)	η	L_M (m)
OS	OE	0.50	0.18	5.79	[5.90]	7.47	[7.60]	19.3	[20.0]	20.4	427	[441]	449	1.05	0.56
	SE		0.18	5.85	[5.98]	7.54	[7.71]	18.9	[19.7]	20.2	357	[435]	444	1.24	0.57
SO	OE	0.50	0.09	3.73	[3.78]	4.81	[4.87]	30.4	[31.2]	31.6	687	[687]	696	1.01	0.49
	SE		0.09	3.73	[3.79]	4.81	[4.88]	30.2	[31.1]	31.6	568	[686]	696	1.23	0.49
SOR	OE	0.25	0.10	3.99	[4.06]	5.15	[5.23]	28.1	[29.1]	29.5	761	[640]	651	0.86	0.32
	SE		0.10	4.00	[4.07]	5.15	[5.25]	28.0	[29.0]	29.5	546	[639]	650	1.19	0.32
LO	OE	0.50	0.34	8.88	[9.15]	11.45	[11.79]	12.2	[12.9]	13.3	279	[284]	293	1.05	0.63
	SE		0.35	8.94	[9.26]	11.52	[11.93]	11.9	[12.7]	13.2	246	[281]	291	1.18	0.64
LOR	OE	2.00	0.32	8.54	[8.83]	11.01	[11.39]	12.5	[13.4]	13.8	246	[294]	304	1.24	1.00
	SE		0.33	8.66	[8.92]	11.16	[11.50]	12.5	[13.2]	13.6	227	[291]	300	1.32	1.02

Table 5: Bulk flow and room averaged results for the different simulations, the simulations described above correspond to the original vent set-up (OS). A^* is calculated from the flow rate and integral of buoyancy obtained in the simulations following eq. (8). Predicted values using the calculated values for c_l and c_h (given in Appendix B) are shown in square brackets. ΔT_e and ΔC_e are calculated based on the measured flow rate assuming a well-mixed environment as described in §3. η is a measure of the contaminant removal efficiency. L_M is the jet-length, characteristic of the rise height of the fountain that forms at the low-level vent

In general, a larger flow rate leads to lower mean CO₂ concentration; this is just one factor that leads to higher values for the opposite-ended configuration in all cases. The contaminant removal efficiency η metric is calculated leading to similar results to the original set-up (OS) for the smaller and larger openings cases where the vent area ratio is kept the same (SO and LO); i.e. a value close to unity for the opposite-ended configuration and a value close to 1.2 for the single-ended configuration. For the cases where the vent area ratio is altered (SOR and LOR), however, this is not the case — this is despite similar flow rates to those of the smaller and larger openings cases (SO and LO), respectively, being achieved with identical effective areas. In the opposite-ended configuration, the set-up with smaller openings and vent area ratio (SOR) has an efficiency well below unity which indicates the increased presence of stagnation zones in the classroom and, further, should the room averaged CO₂ concentration be used to predict the ventilation provision, the rate would be underestimated. For the set-up with larger openings and vent

area ratio (LOR), on the other hand, the values of ventilation efficiency are elevated, in both configurations above 1.2. The flow structure that arises in both cases is discussed below but already this analysis highlights that the effective area A^* and the heat load are not always adequate to predict appropriate estimates of the mean CO_2 and resulting contaminant removal efficiency; instead, in our case, at least the vent area ratio must also be accounted for.

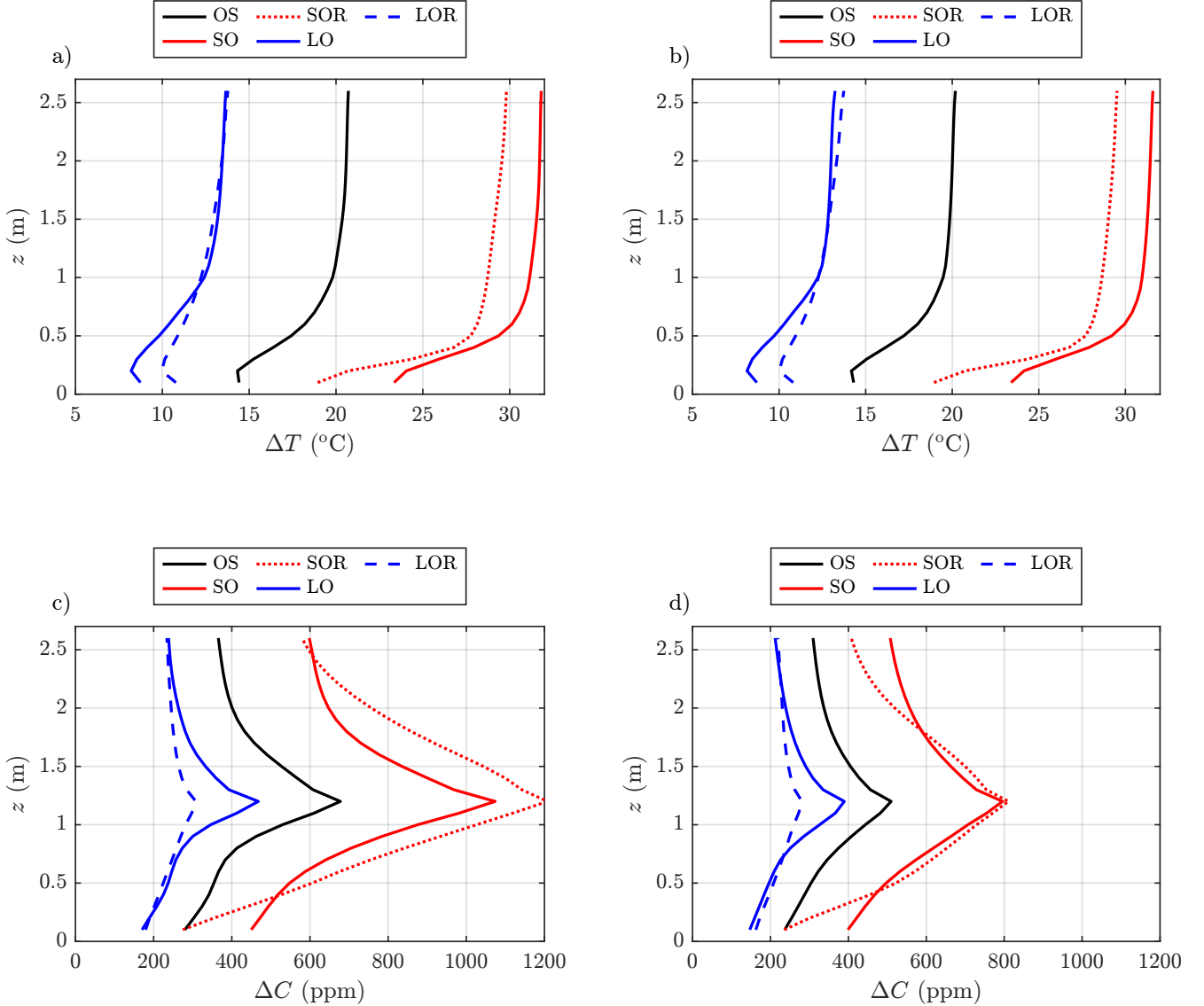


Figure 8: Comparison of the horizontally averaged excess temperature (top panes) and CO_2 concentration (bottom panes) in the classroom for different vent set-ups using the opposite-ended (left panes) and single-ended (right panes) configurations.

The horizontally averaged excess temperatures and CO_2 concentrations are plotted in Figure 8. Trends are similar to those observed in the original vent set-up (OS) for the CO_2 profiles shown in Figure 8c) and Figure 8d), with a significant increase in CO_2 concentration observed for the different opposite-ended configurations when compared to the respective single-ended set-ups. Two notable exceptions are observed. Firstly, the CO_2 concentration in both simulations in the set-up with larger openings and vent area ratio (LOR) varies significantly less across the height of the classroom than what is observed for the simulations with larger openings and the original vent area ratio (LO); although the concentration is similar low down ($z \lesssim 0.8$ m) and high up ($z \gtrsim 2.2$ m), the CO_2 concentration in the breathing zone is considerably lower in the simulations where the vent area ratio is increased (LOR) when compared to those where it is kept the same as the original set-up (LO). Secondly, the CO_2 concentration in the simulations

with smaller openings and vent area ratio (SOR) peaks above all other simulations within the breathing zone but the concentration near the floor is smaller than that of some other scenarios. Qualitatively the temperature profiles shown in Figure 8a) are close to those in Figure 8b), i.e. those for the opposite-ended configurations are broadly similar to those of the single-ended configurations. As expected, increasing the vent areas leads to a decrease in the room temperature (clearly indicated by the room averaged temperature in Table 5) in the set-ups with larger openings (LO and LOR). However, due to the increased vent area ratio, the temperature in the lower third of the room is higher in the LOR case than for the larger openings case with the original vent area ratio (LO). In the smaller openings cases (SO and SOR), on the other hand, changing the vent area ratio has an effect over the entire height of the room, with lower temperatures found in the set-up where the vent area ratio is halved (SOR) when compared to the one with original vent area ratio (SO).

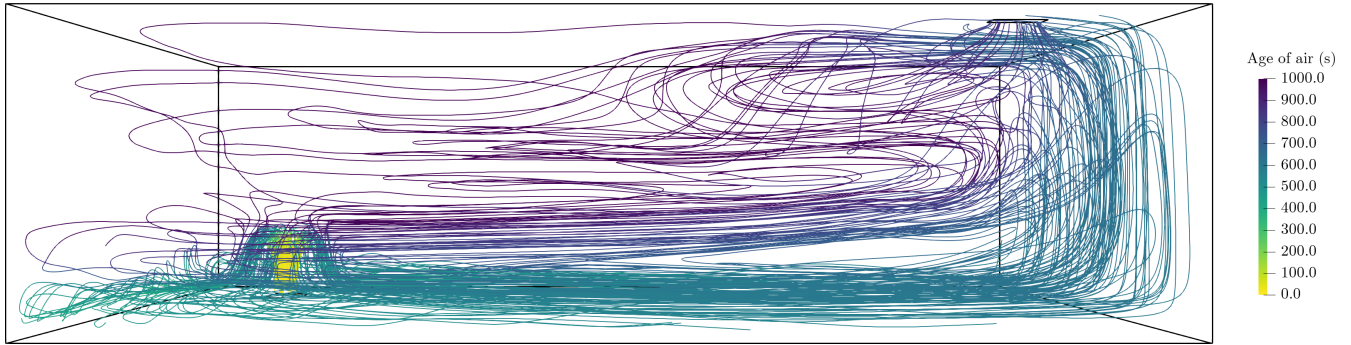
The ventilation patterns in the opposite-ended configuration for the set-ups where the vent area ratio is modified (SOR and LOR) are studied further by looking at the streamlines in each case plotted in Figure 9 and compared to the equivalent smaller and larger openings set-ups with the original vent area ratio (SO and LO). These can be directly compared to Figure 3a), which shows the streamlines for the original vent set-up (OS), also in the opposite-ended configuration. OS, SOR and LOR have identical inlets and heat input, their only difference being the area of the high-level vent leading to different vent area ratios and effective areas. By keeping the low-level vent area constant, the effect of the change in ventilating flow rate can be seen directly. Some of the differences in the mixing that arise within the classroom can be examined through the lens of the mixing induced by the fountain that forms as cooler air rises from the lower vent. For such flows the mixing induced is known to scale with products of the source volume flux, in our case the ventilation flow rate, and powers of the source Froude number Fr [36], see Appendix B for details including the values attained in each simulation. Moreover, the vertical extent over which such mixing is induced is constrained by the rise height of the fountain which is known to be a product of the physical length scale of the source and powers of the source Froude number [37], or in the simplest case their linear product, i.e. the jet-length. As discussed by Hunt and Burrige [35], these findings hold for fountains formed at rectangular sources, such as the vents in our simulations and so we define jet-length as $L_M = \sqrt{A_I} Fr$. With a low flow rate, in the case with smaller openings and vent area ratio (SOR) case, the fountain rises significantly less than the original vent (OS) or the smaller openings set-up with the original vent area ratio (SO), as expected based on the shorter jet-length, and this creates a much larger stagnating zone, with very stale air as indicated by the old age of air and higher CO_2 concentrations observed in Figure 8. In the case with larger openings and vent area ratio (LOR) however, the increase in ventilating flow rate also increases the height of the fountain at the inlet which rises more than halfway across the height of the classroom, much higher than the set-up with similar larger openings but with the original vent area ratio (LO) although the ventilating flow rate is comparable. This encourages recirculation and mixing within the room and no clear stagnation zones are visible. Instead, the streamlines cover most of the classroom and the air is a lot fresher overall, leading to age of air values close to 400s, half of what can be observed in the original vent set-up (OS) and the set-up with smaller openings and vent area ratio (SOR), and further explains the low CO_2 concentrations observed in Figure 8. For both cases where the vent area ratio is different from the original vent set-up (SOR and LOR) considered here, the contaminant removal efficiency is useful to identify cases which do not match previous patterns and which require further investigation.

4.2. CO_2 spatial distribution

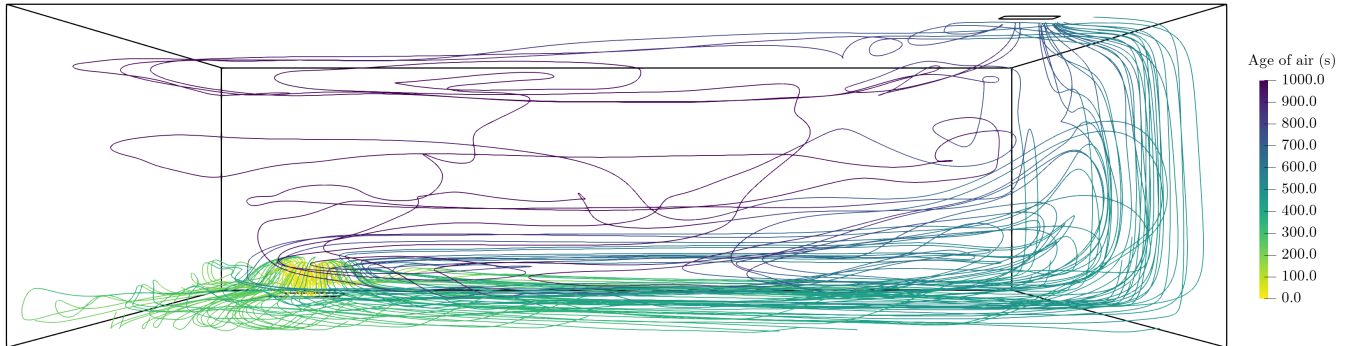
The impact of the changes in scenario on the CO_2 concentration in the room is summarised by the box plots shown in Figure 10. This plot compares the classroom CO_2 distribution in each vent set-up for both the opposite-ended and single-ended configurations.

Figure 10 shows that the values of CO_2 in the classroom are consistently lower in the single-ended configurations, often accompanied by lower spreads in the measured values. For similar geometries, the spread and overall CO_2 in the room increases as the flow rate decreases. The differences between the opposite-ended and single-ended distributions reduce as the ventilating flow rate increases, better agreement is seen for instance for the set-ups with larger openings (LO and LOR). As identified above, the case with smaller openings and vent area ratio (SOR) displays the highest spread in CO_2 concentrations, with values ranging from the ambient 400 ppm to over 2,000 ppm in the opposite-ended configuration, although its median is similar to the the other set-up with smaller openings (SO). The increased mixing observed for the case with larger openings and vent area ratio (LOR) is also demonstrated with a smaller spread in CO_2 concentrations.

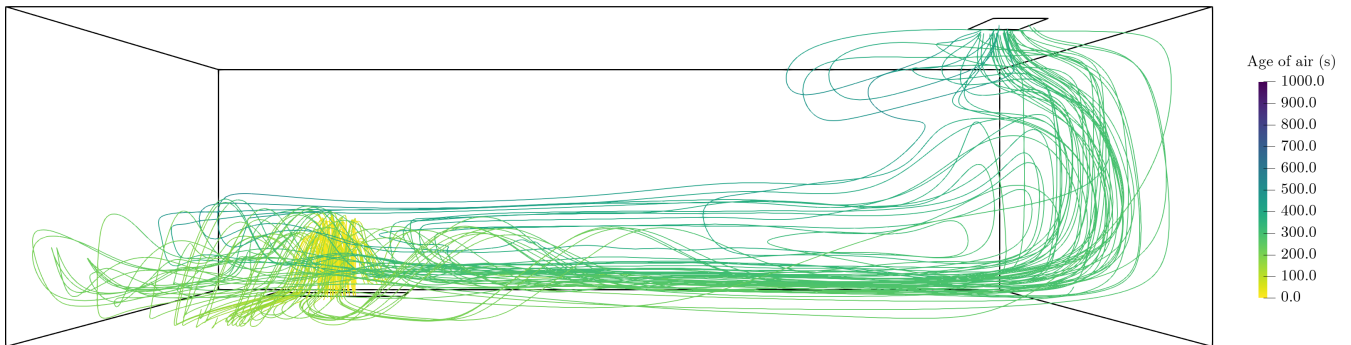
a) SO



b) SOR



c) LO



d) LOR

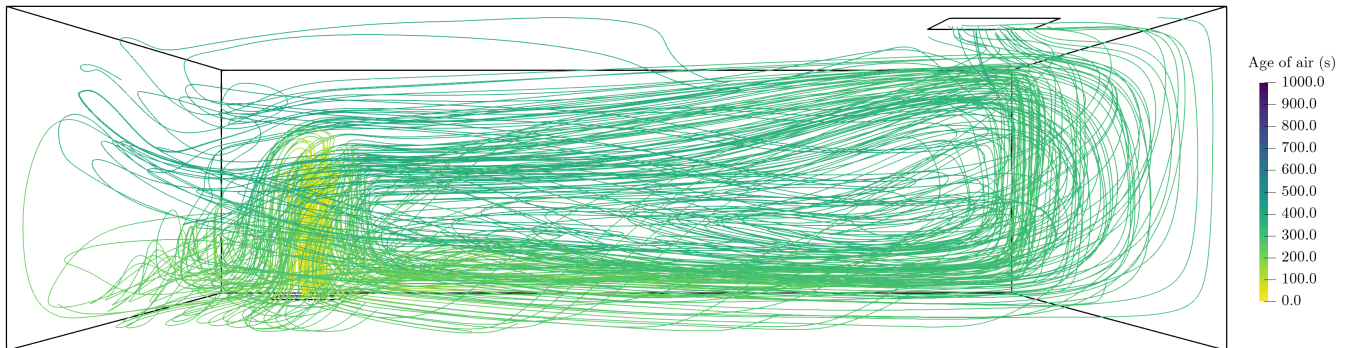


Figure 9: Streamlines originating from the low-level vent in the opposite-ended configuration for a) the SO, b) SOR, c) LO and d) LOR cases coloured by the age of air. In both cases, 100 streamlines are seeded at the classroom inlet.

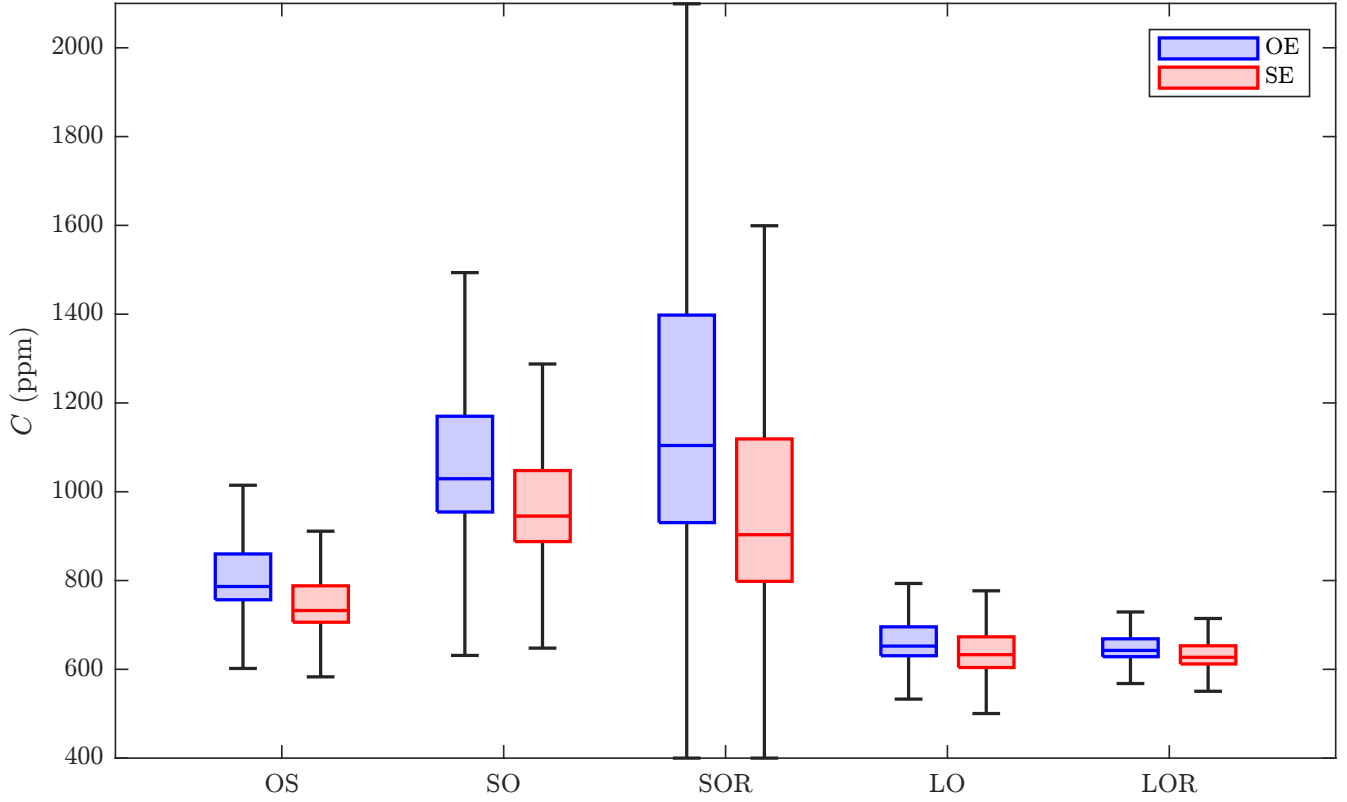


Figure 10: CO₂ distribution in the classroom for different vent set-ups in the opposite-ended (blue) and single-ended (red) configurations. The bottom and top of the box show the 25th and 75th percentiles, the median is shown by the central horizontal line. The whiskers include data within one and a half of the interquartile range from the 1st and 3rd quartiles.

4.3. Sensor placement

Figure 11 presents the scale of the expected errors in the predicted mean using wall measurements, ϵ , and the coefficient of variations found using the measurement over the entire height $cVar$ and at the walls only $cVar_w$ for all of the scenarios examined. This is shown for the two heights which show the largest differences in §3.4: $z = 1.1$ m and $z = 1.9$ m. As shown previously, the error and coefficients of variations are larger near the breathing zone, which can be expected. Agreement between wall measurements and those over the entire plane are closer higher up within the classroom for all cases, with errors in the predicted mean ranging from less than 1% to 4% (coefficients of variation varying between 1% and 8% in the domain and 1% and 12% at the walls). This is small compared to the uncertainty associated with CO₂ measurements which is typically taken to be ± 50 ppm or 3% of the reading. All parameters show distinct peaks at 1.9 m in the opposite-ended configuration for the smaller opening scenarios (SO, SOR) which are found to have a larger spreads in the CO₂ distributions therefore leading to higher errors and coefficient of variations. In the breathing zone ($z = 1.1$ m), trends are not as clear, the error ϵ ranges from 1% to 12% over the different set-ups, with the single-ended configuration leading to better results (and a smaller error) in all but 2 cases (SO and LO). In both ventilation configurations, the maximum error is reached for the case smaller openings and vent area ratio (SOR). At $z = 1.1$ m, the coefficients of variation vary between 9% and 25% in the domain and 9% and 29% at the walls, with consistently higher values for the opposite-ended configuration. Here, a significant decrease in the coefficient of variation is visible for the simulation with larger openings and vent area ratio (LOR), which is explained by the increased recirculation and mixing in the room observed in Figure 9d).

Across the different simulations considered here, wall measurements are found to be more accurate at points higher in the room. The CO₂ distribution in the breathing zone displays larger variations for all set-ups and would be hard to measure accurately with a limited number of sensors. Despite significant changes in the ventilation pattern created by changes in the vent areas and ratio, conclusions drawn for the original vent set-up hold up for the different vents considered. Larger variations of CO₂ are observed using the opposite-ended configuration and wall measurements taken above the breathing zone and below the high-level vent are found to be the most accurate

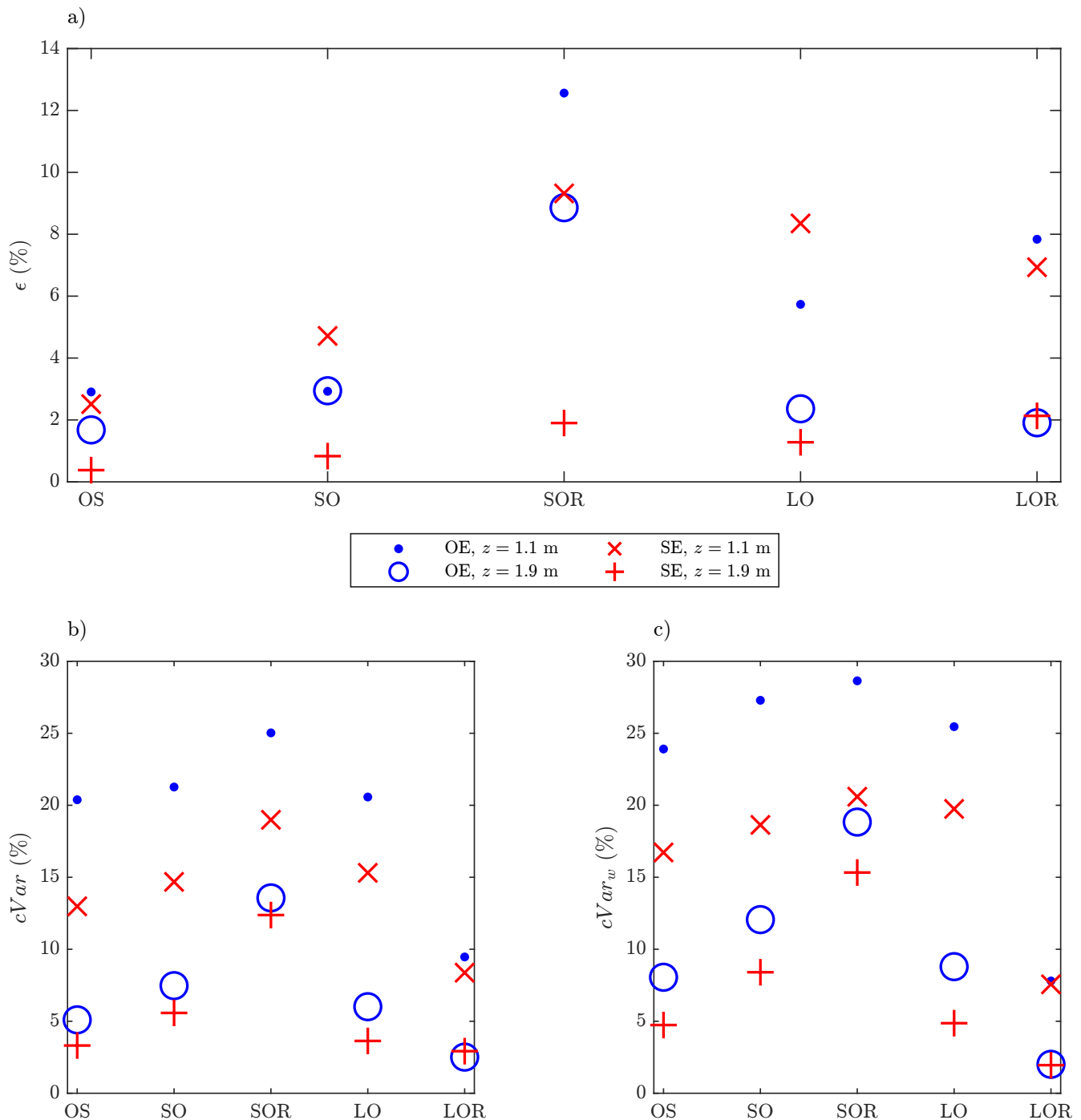


Figure 11: Accuracy of the CO₂ measurements at the walls at $z = 1.1$ m and $z = 1.9$ m for the different vent set-ups. Results for both the opposite-ended and single-ended configurations are shown. ϵ is the error in the predicted mean when considering the CO₂ concentration near the walls (defined as within 0.2 m of a wall). $cVar$ is coefficient of variation of the CO₂ concentration over the whole room at a given height and $cVar_w$ quantifies the coefficient of variation at the same height considering measurements near the walls only.

to represent the distribution at that height.

5. Inference of ventilation rates

Following the simulations presented under steady state, an estimate of the ventilation rate Q_E can be determined by rearranging eq. (7) based on the CO₂ measurement, C , at any point within the room, giving

$$Q_E = \frac{N G}{C - C_a}. \quad (3)$$

The error within the estimated ventilation rate Q_E is therefore determined by the inaccuracies in the measured or estimated values of the other parameters; namely the source term (here expressed as a product of the occupancy, N , and the mean production rate per person, G), and the difference between the measured carbon dioxide, C and the ambient CO₂, C_a . We aim to establish how the uncertainty induced by spatial variations of measured CO₂, C , compare to the magnitude of the uncertainties due to the other three parameters. For instance, although 32 occupants is a standard number for UK classrooms, occupancy levels can be difficult to obtain in practice and so often this number has to be estimated and it might be realistic to assume that N can vary by ± 5 occupants across classrooms. The individual CO₂ generation rate, G is also extremely variable, depending both on the population and their activity. The value used in this paper ($3.35 \times 10^{-6} \text{ m}^3/\text{s}$) is obtained from Persily and de Jonge [23] and is already a population average based on body mass distribution. Although this distribution can have a significant spread, the standard deviation will reduce (statistically by a factor statistically expected to be \sqrt{N}) when averaging over N occupants. However, their level of activity remains a vital factor. Herein the activity level is assumed to be 1.4 met corresponding to the activity levels of a sitting office worker but it can be reasonable to assumed to vary between 1.2 met (sitting quietly) and 1.6 met (office worker moving around) in a classroom. This in turn means that G for primary school aged children aged between 6 and 11 could vary between $2.7 \times 10^{-6} \text{ m}^3/\text{s}$ (taking 1.2 met and young female students to be present) and $4.0 \times 10^{-6} \text{ m}^3/\text{s}$ (taking 1.6 met and older male students to be present) [23]. Finally, there is also an uncertainty associated with the outdoor CO₂ level C_a used to estimate the excess CO₂ concentration, which can be assumed to reasonably vary by ± 50 ppm.

The distribution of the estimated flow rate, Q_E (based on the distribution of measurement points of $C(x, y, z)$ obtained from the simulations), is illustrated in Figure 12 by curves representing the mean and the quartiles in the distribution of the normalised metric Q_E/Q , where Q is actual ventilation flow rate measured within the simulations. Along the horizontal axes within Figure 12, the other three parameters are varied to ultimately provide an illustration of the sensitivity of ventilation rates inferred from point measurements, i.e. Q_E/Q , relative to other sensitivities associated with classroom operation. In Figure 12a) the estimated source term $N_E G_E$ is varied and normalised by the source term within the simulations, i.e. NG ; in Figure 12b) the estimated value of the outdoor concentration C_{aE} is varied and normalised by C_a , the outdoor concentration defined in §2. The CO₂ concentrations measured (at all locations within the room) are taken from the original vent set-up simulations (OS). Within Figure 12 thin solid curves mark the data of the estimated ventilation rate taking the room averaged CO₂ concentration, i.e. $C = \langle C \rangle$ within eq. (3); by construction, these thin curves pass through the points $(1, \eta)$ with the contaminant removal efficiency being $\eta = 1.05$ for the opposite-ended configuration, and $\eta = 1.24$ for the single-ended. Thick solid curves within Figure 12 show the estimated ventilation rate using the median CO₂ concentration and dashed curves mark the estimates using the CO₂ concentrations corresponding to the 1st and 3rd quartiles of the distributions (see Figure 6a) for histograms of these distributions). All remaining parameters are kept constant and equal to the values described in §2.

Figure 12 shows that the estimation of the ventilation rate can vary greatly depending on the particular location of the CO₂ concentration used. Considering the interquartile range within the base-case OS, i.e. taking $N_E G_E / NG = 1$ or $C_{aE} / C_a = 1$, variations in the location of the CO₂ measurement lead to estimations of the ventilation rate that vary by around $\pm 15\%$ about the median value. However, Figure 12 also shows that the uncertainty introduced by the other parameters in eq. (3) also significantly affects estimates of the ventilation rate. This is particularly significant for the source term $N_E G_E$ (Figure 12a) for which, independent variation over the range considered, leads to variations in the estimated ventilation rate varies by up to 70%. In the case of the outdoor concentration (Figure 12b), independent variation over the range ± 50 ppm, results in estimations varying by 35%. These results highlight that even though the location of CO₂ measurements is indeed important when estimating ventilation rates, the accuracy of these estimates depends strongly on other parameters too; parameters that are, all too often, overlooked and, in the case of the source term, are impractical to measure.

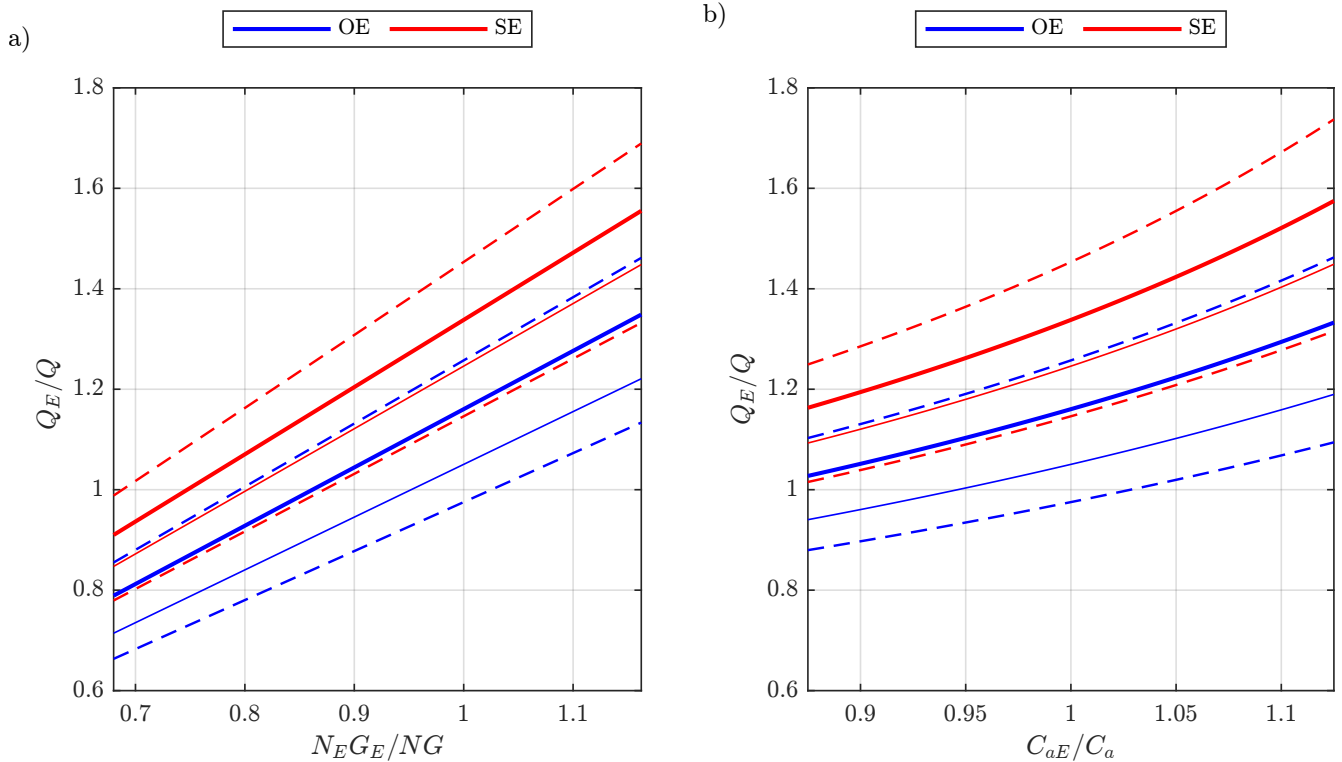


Figure 12: Sensitivity of the estimated ventilation rate to: a) the normalised source term $N_E G_E / N G$ and b) the normalised outdoor CO_2 concentration C_{aE} / C_a . $N G$ and C_a are the respective values of the source term and ambient CO_2 concentration used in the numerical simulations and defined in §2. For each case, the estimated ventilation rate Q_E is normalised by the flow rate Q achieved in numerical simulation for the original vent set-up (OS), either in the opposite-ended (OE) or single-ended (SE) configuration (given in Table 2). Thick solid curves show the ventilation rate obtained by using the median CO_2 concentration achieved in each configuration, thin solid curves show the estimates when taking the room averaged CO_2 concentration and the dashed curves show the rate estimated by using the concentrations corresponding either to the 1st or 3rd quartiles of the distribution (as plotted in Figure 6a). For each parameter, the variation in the calculated flow rate is shown for the expected range of variations defined in §5.

6. Conclusion

Significant spatial variations in the CO_2 concentration were observed in all the ventilation set-ups considered in this study, and consideration of their implications have been presented. It was shown that these spatial variations in the CO_2 concentration result in the precise location of measurements being an important factor to consider when inferring metrics concerning the ventilation. However, uncertainties, e.g. in estimating the scale of the source term, have been shown to be at least as important as the choice of measurement location. Moreover, when reporting ventilation metrics, one must consider the most appropriate rate to report; for example, whether one is trying to report metrics of the bulk ventilation rate (i.e. the volume flux of air exchanged with outdoors) or report metrics of the effectiveness of the ventilation for occupants. These differ by a factor, related to the contaminant removal efficiency, which varies considerably depending on the given ventilation configuration. Practically, there remains questions as to how frequently measurements in classrooms might be deemed to approximately represent steady state CO_2 concentrations, this is especially the case when air change rates are low (either due to ventilation rates being low or room volumes being relatively large). If one takes peak CO_2 concentrations to be representative of the steady value, as has been the case in some previous field studies [e.g. 1], then the ventilation provision is likely to be inherently overestimated.

In the configurations presented, the spatial distribution of CO_2 and resulting contaminant removal efficiency was shown to depend both on the relative horizontal position of the vents as well as the ratio of the vent areas. When the low-level inlet, and high-level outlet, vents were positioned at one end of the classroom (single-ended configuration) the ventilation strategy was shown to be most efficient, consistently leading to lower CO_2 concentrations in the classroom. Changes to the ratio of the vent areas also led to changes in the mixing induced by the fountain created at the low-level vent. This highlights that in addition to the effective area, the relative position of the vents and the

ratio of their areas need to be carefully considered to determine the effectiveness of the ventilating flow established, and the resulting CO₂ concentration in spaces designed to promote buoyancy driven ventilation.

Relevant to the choice of location for CO₂ measurements to be made, herein the variations of CO₂ were shown to be highest within the breathing zone ($1 \leq z \leq 1.5$ m) with the spread in the observed concentration decreasing at greater heights due to the vertical displacement flow established. Measurements near the walls (within 0.2 m) were compared to the distribution found over the whole room at each height. This is pertinent in classrooms, as sensors are often placed out of the way and fixed to walls. This comparison shows that, for ventilation strategies which promote low-level inflows and high-level outflows, sensors placed near walls can be useful to predict the mean CO₂ at that height, provided they are above the breathing zone and below the classroom ventilation outlet. CO₂ measurements should however be used with caution when used to infer ventilation rates, even if they are broadly representative of the mean CO₂. In the single-ended configuration, for instance, where the contaminant removal efficiency is superior to unity (unity being the well-mixed efficiency), calculating the ventilation flow rate from the room averaged CO₂ would lead to overestimating the actual ventilation supply by 25%. The robustness of these results was investigated by considering a range of scenarios in which the ventilating flow rate was varied either by changing the opening areas or the ratio of their areas. As expected, a lower flow rate leads to higher CO₂ concentrations, but, crucially, also lead to higher variations in the concentration within the classroom.

The deployment of CFD simulations, with boundary conditions far removed from the room inlet and outlet vents, enabled the simulation of a naturally ventilated classroom in which the flow rate is set naturally by the heat input and not imposed at the vents. This allowed for the independent calculation of the discharge coefficients at each vent which is often challenging to achieve experimentally (see Appendix B). We hope this might inspire further study since parameterisations of the losses at the vents are key in the design of natural ventilation [38]. In particular, it would be interesting to determine how the results presented herein are impacted when vents are placed vertically on walls, as is typical of windows. It must also be noted that this study assumed convection to be the dominant mechanism of heat transfer and as such the effects of thermal radiation and conduction were not explicitly modelled. Radiation acts to redistribute heat, from warmer to cooler surfaces, within rooms and conduction typically lessens the total net heat load (via heat losses through the building fabric). The inclusion of these mechanisms is likely to impact the vertical temperature distribution, potentially weakening the thermal stratification and lowering any fluid velocities associated with the buoyancy due to temperature differences. Thus, a useful extension of this work would be to include these effects to determine whether they are expected to significantly affect the findings presented herein, although the computational cost of doing so should not be underestimated.

This work shows that considerable variations in CO₂ can be expected even in idealised naturally ventilated classrooms, even in the limiting case that the heat loads are well distributed. Predictions of concentrations based on the well-mixed assumption should be used with caution, ideally alongside account of the expected variations. If the goal is to estimate the overall ventilation rate, CO₂ measurements taken above the breathing zone were shown to be most accurate for the configurations examined. Irrespective, when metrics of the ventilation are being inferred from point measurements of the CO₂ concentration, the particular measurement location has been highlighted to be just one important factor to consider, and is often not the most important consideration.

Acknowledgements

We gratefully acknowledge Fred Mendonça and his team at OpenCFD for providing support and advice on setting up the numerical simulations. CVMV was funded via the Imperial College London Centres for Doctoral Training in Fluid Dynamics Across Scales [grant EP/L016230/1] and the School Air quality Monitoring for Health and Education SAMHE project [grant EP/W001411/1]. Computational resources were provided by the UK Turbulence Consortium [grant EP/R029326/1].

Competing interests

The authors declare no competing interests.

Appendix A Well-mixed predictions

The limiting case that the air within the classroom is perfectly mixed and all properties of the air are uniformly distributed throughout the volume, the so-called ‘well-mixed’ approximation, provides predictions for the room averaged temperature T_c , CO₂ concentration C_c and ventilation flow rate Q_c . These predictions are based on the work of Gladstone and Woods [29] who used a distributed heat source. Such predictions, by their very nature, are unaffected by the horizontal locations of the ventilation openings and are identical for the opposite-ended and single-ended configurations. The expected volume flow rate is

$$Q_c = A^{*2/3} \left(\frac{g \alpha}{\rho_a c_p} \right)^{1/3} W_c^{1/3} H_c^{1/3}, \quad (4)$$

where g is the gravitational acceleration, α the thermal expansion coefficient, ρ_a the ambient density, c_p the specific heat capacity, W_c the heat input to the room and H_c is the classroom height. The different parameters and their respective values are summarised in Table 1. The effective vent area A^* characterises both vent areas and the effect of flow contraction at the openings and is defined as

$$A^* = \frac{\sqrt{2} c_l A_l c_h A_h}{\sqrt{(c_l A_l)^2 + (c_h A_h)^2}}, \quad (5)$$

where A_l and A_h are the bottom and top vent areas respectively. The discharge coefficients c_l and c_h are the discharge coefficients at the low- and high-level vents, their calculation is detailed in Appendix B. The resulting room temperature T_c is given by

$$T_c = T_a + W_c^{2/3} (\rho_a c_p A^*)^{-2/3} (g \alpha, H_c)^{-1/3}, \quad (6)$$

where T_a is the ambient temperature. The steady state classroom CO₂ concentration is given by

$$C_c = \frac{N G}{Q_c} + C_a, \quad (7)$$

with N the number of occupants, G their respective CO₂ generation rate and C_a the ambient CO₂ concentration, typically expressed in ppm.

Appendix B Independent calculations of the discharge coefficient at each vent

Theoretical predictions and experimental data evidence the need to characterise the energy losses at the vents. As is standard, we parameterise these losses via discharge coefficients. From the simulated data, the effective area can be evaluated from

$$A^* = \frac{Q}{(\int_0^{H_c} g' dz)^{1/2}}, \quad (8)$$

where the ventilation flow rate, Q , and the buoyancy integral, $\int_0^{H_c} g' dz$ can be determined from the CFD results. Rearranging eq. (5) and assuming $c_l = c_h = c_d$ as done typically, the discharge coefficient can be determined as

$$c_d = \frac{A^*}{\sqrt{2} A_l A_h} \sqrt{A_l^2 + A_h^2}. \quad (9)$$

B.1 Changes in the discharge coefficient with configuration

The value for both configurations is given in Table 6. In both cases it is close to 0.7, and so lies within the experimentally determined range of $0.6 \leq c_d \leq 1.0$ [29, 30].

The assumption of an identical discharge coefficient at each vent can be relaxed by assessing numerically the neutral pressure level z_{npl} , the height at which the pressure in the room is equal to the ambient pressure. Then, the ratio

$$R^* = \frac{A_l c_l}{A_h c_h}, \quad (10)$$

can be found, following the work of [39] and [40], from

$$R^* = \sqrt{\frac{H_C}{z_{npl}} - 1}. \quad (11)$$

Rearranging eq. (5), the discharge coefficient at the low-level vent can be determined from:

$$c_l = \frac{A^*}{A_l} \sqrt{\frac{R^{*2} + 1}{2}}, \quad (12)$$

and c_h is obtained by rearranging eq. (10). The results for both configurations are summarised in Table 6, alongside the discharge coefficients c_d obtained when c_h is assumed to be the same as c_l . The table also gives the Reynolds number, calculated at each vent with area A :

$$Re = \frac{Q}{\nu A^{1/2}}, \quad (13)$$

where the kinematic viscosity is $\nu = 1.37 \times 10^{-5}$ m²/s, and the Froude number:

$$Fr = \frac{Q^{3/2}}{F_s^{1/2} A^{5/4}}, \quad (14)$$

where F_s is the source buoyancy flux, found from the distributed heat input with $F_s = \alpha g W_C / (\rho c_p)$. We note that eq. (13) and eq. (14) arise upon taking the characteristic scale of the momentum flux at the vent to be $M = Q^2/A$. At the high-level vent $Fr_h = Fr$ and the low-level vent $Fr_l = -Fr$ due to the opposing buoyancy force.

	A^* (m ²)	c_d	c_l	c_h	Re_l	Re_h	Fr_l	Fr_h
Opposite-ended simulation	0.18	0.69	0.52	0.77	2.75×10^4	3.89×10^4	-0.88	2.10
Single-ended simulation	0.18	0.71	0.52	0.80	2.78×10^4	3.93×10^4	-0.90	2.13

Table 6: Effective area A^* and discharge coefficients obtained numerically for each ventilation configuration. c_d is obtained by assuming the loss coefficient is the same at each vent, c_h and c_l give the high- and low-level vent discharge coefficient respectively after considering the neutral pressure level. Re_l and Re_h give the Reynolds number, Fr_l and Fr_h the Froude number at the low- and high-level vents respectively.

Table 6 shows that the losses due to contraction at the low-level vent are more significant than at the high-level vent for both ventilation configurations. At the low-level vent, both the Reynolds number and the magnitude of the Froude numbers are lower than at the high-level vent. However, the flow at all vents remains sufficient to be regarded as high-Reynolds number, i.e. the flow is expected to be independent of Reynolds numbers [41]. Given this, and the fact that at both low- and high-level vents the flow experiences both a significant contraction then expansion, our findings may be suggestive that change in sign of the Froude number, i.e. the flow beyond the low-level vent forms a fountain and beyond the high-level vent a plume, plays a significant role in determining the losses at the vent. We note that far less is known about the dependence of the losses at vents due to buoyancy effects, as characterised by the Froude number, than Reynolds number — this identifies an outstanding challenge.

In addition, apparent increases in the discharge coefficient at the high-level vent, c_h , are evident for the single-ended configuration — the reasons for this are not clear. The calculation of specific discharge coefficients at each vent requires pressure differences to be measured, this is challenging experimentally — something numerical simulations are well placed to address.

B.2 Changes in the discharge coefficient with vent area

The discharge coefficients, Reynolds numbers, and Froude numbers are also calculated for the simulations discussed in §4, and are presented in Table 7. This shows that the discharge coefficient at the low-level vent, c_l , remains low, relative to c_h , in all cases; supporting the suggestion that buoyancy effects across the vents may be important in determining the losses. Moreover, c_l remains equally low for both the single- and opposite-ended configuration in all of the cases examined. This does not remain true for c_h , where a lower value is often found in the opposite-ended configuration. Changes due to variations in the vent areas are most visible at the low-level. Whilst c_h remains within the range 0.74–0.8 for all the cases considered, c_l varies more widely (0.46–0.62), reaching a minimum for the case with smaller openings and vent area ratio (SOR) and a maximum for the set-up with larger openings and vent area ratio (LOR).

Case	Vents	A_h/A_l	A^* (m ²)	c_l	c_h	Re_l	Re_h	Fr_l	Fr_h
OS	OE	0.50	0.18	0.52	0.77	2.8×10^4	3.9×10^4	-0.88	2.10
	SE		0.18	0.52	0.80	2.8×10^4	3.9×10^4	-0.90	2.13
SO	OE	0.50	0.09	0.55	0.78	2.5×10^4	3.5×10^4	-1.09	2.58
	SE		0.09	0.55	0.78	2.5×10^4	3.5×10^4	-1.09	2.58
SOR	OE	0.25	0.10	0.46	0.77	1.9×10^4	3.8×10^4	-0.51	2.86
	SE		0.10	0.46	0.77	1.9×10^4	3.8×10^4	-0.51	2.87
LO	OE	0.50	0.34	0.51	0.74	3.0×10^4	4.2×10^4	-0.70	1.68
	SE		0.35	0.51	0.76	3.0×10^4	4.2×10^4	-0.71	1.69
LOR	OE	2.00	0.32	0.62	0.74	4.1×10^4	2.9×10^4	-1.58	0.66
	SE		0.33	0.62	0.80	4.1×10^4	2.9×10^4	-1.61	0.68

Table 7: Effective area A^* and discharge coefficients at each vent calculated for each set-up. Re_l and Re_h are the Reynolds numbers, and Fr_l and Fr_h are the Froude numbers at the low- and high-level vents respectively.

References

- [1] U. Haverinen-Shaughnessy, D. J. Moschandreas, R. J. Shaughnessy, Association between substandard classroom ventilation rates and students’ academic achievement, *Indoor Air* 21 (2011) 121–131. doi:10.1111/j.1600-0668.2010.00686.x.
- [2] L. Chatzidiakou, D. Mumovic, A. J. Summerfield, What do we know about indoor air quality in school classrooms? A critical review of the literature, *Intelligent Buildings International* 4 (2012) 228–259. doi:10.1080/17508975.2012.725530.
- [3] T. Salthammer, E. Uhde, T. Schripp, A. Schieweck, L. Morawska, M. Mazaheri, S. Clifford, C. He, et al., Children’s well-being at schools: Impact of climatic conditions and air pollution, *Environment International* 94 (2016) 196–210. doi:10.1016/j.envint.2016.05.009.
- [4] W. J. Fisk, The ventilation problem in schools: literature review, *Indoor Air* 27 (2017) 1039–1051. doi:10.1111/ina.12403.
- [5] A. K. Persily, Field measurement of ventilation rates, *Indoor Air* 26 (2016) 97–111.
- [6] ISO, ISO 12569 Thermal Performance of Buildings and Materials—Determination of Specific Airflow Rate in Buildings—Tracer Gas Dilution Method, International Organization for Standardization, 2017.
- [7] S. Batterman, Review and extension of CO₂ -based methods to determine ventilation rates with application to school classrooms, *International journal of environmental research and public health* 14 (2017) 145.
- [8] A. Kabirikopaei, J. Lau, Uncertainty analysis of various CO₂ -based tracer-gas methods for estimating seasonal ventilation rates in classrooms with different mechanical systems, *Building and Environment* 179 (2020) 107003.

- [9] A. K. Persily, Evaluating building iaq and ventilation with indoor carbon dioxide, *Transactions-American society of heating refrigerating and air conditioning engineers* 103 (1997) 193–204.
- [10] ASHRAE, ASHRAE position document on indoor carbon dioxide, American Society of Heating, Refrigerating and Air-Conditioning Engineers, 2022.
- [11] D. Zhang, E. Ding, P. M. Bluyssen, Guidance to assess ventilation performance of a classroom based on CO₂ monitoring, *Indoor and Built Environment* 31 (2022) 1107–1126.
- [12] N. Mahyuddin, H. B. Awbi, M. Alshitawi, The spatial distribution of carbon dioxide in rooms with particular application to classrooms, *Indoor and Built Environment* 23 (2014) 433–448.
- [13] Ministry of Housing, Communities & Local Government, Energy performance of buildings data: England and Wales, 2021. Data retrieved from Energy Performance Certificates, [https://epc.opendatacommunities.org/\[23/09/2021\]](https://epc.opendatacommunities.org/[23/09/2021]).
- [14] O. Seppänen, W. Fisk, M. J. Mendell, Association of ventilation rates and CO₂ concentrations with health and other responses in commercial and institutional buildings, *Indoor air* 9 (1999) 226–252.
- [15] C. V. M. Vouriot, T. D. Higton, P. F. Linden, G. O. Hughes, M. van Reeuwijk, H. C. Burridge, Uniformly distributed floor sources of buoyancy can give rise to significant spatial inhomogeneities within rooms, *Flow* 3 (2023) E18.
- [16] P. F. Linden, G. F. Lane-Serff, D. A. Smeed, Emptying filling boxes: the fluid mechanics of natural ventilation, *Journal of Fluid Mechanics* 212 (1990) 309. doi:10.1017/S0022112090001987.
- [17] G. Hunt, P. Linden, The fluid mechanics of natural ventilation—displacement ventilation by buoyancy-driven flows assisted by wind, *Building and Environment* 34 (1999) 707–720. doi:10.1016/S0360-1323(98)00053-5.
- [18] G. Carrilho da Graça, A technical note on simplified modeling of turbulent mixing in wind-driven single sided ventilation, *Building and Environment* 131 (2018) 12–15. doi:10.1016/j.buildenv.2018.01.014.
- [19] C. V. M. Vouriot, H. C. Burridge, C. J. Noakes, P. F. Linden, Seasonal variation in airborne infection risk in schools due to changes in ventilation inferred from monitored carbon dioxide, *Indoor Air* 31 (2021) 1154–1163. doi:10.1111/ina.12818.
- [20] Department for Education, Building Bulletin 101: Guidelines on ventilation, thermal comfort and indoor air quality in schools, 2018. <https://www.gov.uk/government/publications/building-bulletin-101-ventilation-for-school-buildings> [accessed 23/09/2021].
- [21] Department for Education, Building Bulletin 103: Area guidelines for mainstream schools, 2014. <https://www.gov.uk/government/publications/area-guidelines-and-net-capacity> [accessed 23/09/2021].
- [22] B. Jones, P. Sharpe, C. Iddon, E. A. Hathway, C. J. Noakes, S. Fitzgerald, Modelling uncertainty in the relative risk of exposure to the SARS-CoV-2 virus by airborne aerosol transmission in well mixed indoor air, *Building and Environment* 191 (2021) 107617. doi:10.1016/j.buildenv.2021.107617.
- [23] A. Persily, L. de Jonge, Carbon dioxide generation rates for building occupants, *Indoor Air* 27 (2017) 868–879. doi:10.1111/ina.12383.
- [24] OpenCFD, buoyancyTurbSource finite-volume option, 2020. <https://www.openfoam.com/news/main-news/openfoam-v20-12/solver-and-physics-solver-and-physics-buoyancy-fvoption> [accessed 23/05/2022].
- [25] S. B. Pope, *Turbulent Flows*, Cambridge University Press, Cambridge, UK, 2000. doi:10.1017/CB09780511840531.
- [26] B. Blocken, LES over RANS in building simulation for outdoor and indoor applications: A foregone conclusion?, *Building Simulation* 11 (2018) 821–870. doi:10.1007/s12273-018-0459-3.
- [27] OpenCFD, ESI OpenCFD Release OpenFOAM®v2106, 2021. <https://www.openfoam.com/news/main-news/openfoam-v2106> [accessed 23/05/2022].

- [28] C. V. M. Vouriot, The potential for spatial variations in exposure and infection risk within a typical UK classroom: COVID-19 as a case study, Ph.D. thesis, Imperial College London, 2022.
- [29] C. Gladstone, A. W. Woods, On buoyancy-driven natural ventilation of a room with a heated floor, *Journal of Fluid Mechanics* 441 (2001) 293–314. doi:10.1017/S0022112001004876.
- [30] P. Heiselberg, K. Svidt, P. V. Nielsen, Characteristics of airflow from open windows, *Building and Environment* 36 (2001) 859–869. doi:10.1016/S0360-1323(01)00012-9.
- [31] A. Novoselac, J. Srebric, Comparison of air exchange efficiency and contaminant removal effectiveness as IAQ indices, *ASHRAE Transactions* 109 PART 2 (2003) 339–349.
- [32] G. Carrilho da Graça, P. Linden, Ten questions about natural ventilation of non-domestic buildings, *Building and Environment* 107 (2016) 263–273. doi:10.1016/j.buildenv.2016.08.007.
- [33] M. Sandberg, What is ventilation efficiency?, *Building and Environment* 16 (1981) 123–135. doi:10.1016/0360-1323(81)90028-7.
- [34] ASHRAE, Measuring air-change effectiveness, American Society of Heating, Refrigerating and Air-Conditioning Engineers Standard 129-1997 (RA 2002), 2002. ISSN 1041-2336.
- [35] G. Hunt, H. Burridge, Fountains in industry and nature, *Annual Review of Fluid Mechanics* 47 (2015) 195–220.
- [36] H. Burridge, G. Hunt, Entrainment by turbulent fountains, *Journal of Fluid Mechanics* 790 (2016) 407–418.
- [37] H. Burridge, G. Hunt, The rise heights of low-and high-Froude-number turbulent axisymmetric fountains, *Journal of fluid mechanics* 691 (2012) 392–416.
- [38] CIBSE, AM10 Natural ventilation in non-domestic buildings, CIBSE Publications, 2005.
- [39] O. Connick, The Fluid Mechanics of Hybrid Ventilation, Ph.D. thesis, Imperial College London, 2013.
- [40] O. Connick, G. R. Hunt, Hybrid ventilation of a room: a theoretical model for the combined effects of mechanically-imposed and buoyancy-induced driving pressures, *Building and Environment* 169 (2020) 106546.
- [41] D. Etheridge, *Natural ventilation of buildings: theory, measurement and design*, John Wiley & Sons, 2011.